Available online at www.sciencedirect.com
SCIENCE DIRECT®
Journal of Computational Physics 211 (2006) 719–747
JOURNAL OF COMPUTATIONAL PHYSICS
www.elsevier.com/locate/jcp

A (Dis)continuous finite element model for generalized 2D vorticity dynamics

Erik Bernsen, Onno Bokhove *, Jaap J.W. van der Vegt

Department of Applied Mathematics, Institute of Mechanics, Processes and Control, University of Twente, P.O. Box 217, 7500 AE, Enschede, The Netherlands

Received 9 August 2004; received in revised form 7 June 2005; accepted 8 June 2005
Available online 24 August 2005

Abstract

A mixed continuous and discontinuous Galerkin finite element discretization is constructed for a generalized vorticity streamfunction formulation in two spatial dimensions. This formulation consists of a hyperbolic (potential) vorticity equation and a linear elliptic equation for a (transport) streamfunction. The generalized formulation includes three systems in geophysical fluid dynamics: the incompressible Euler equations, the barotropic quasi-geostrophic equations and the rigid-lid equations. Multiple connected domains are considered with impenetrable and curved boundaries such that the circulation at each connected piece of boundary must be introduced. The generalized system is shown to globally conserve energy and weighted smooth functions of the vorticity. In particular, the weighted square vorticity or enstrophy is conserved. By construction, the spatial finite-element discretization is shown to conserve energy and is L^2-stable in the enstrophy norm. The method is verified by numerical experiments which support our error estimates. Particular attention is paid to match the continuous and discontinuous discretization. Hence, the implementation with a third-order Runge–Kutta time discretization conserves energy and is L^2-stable in the enstrophy norm for increasing time resolution in multiple connected curved domains.

Keywords: Generalized vorticity streamfunction formulation; Multiple connected and curved domains; Discontinuous Galerkin finite elements; Energy conservation and enstrophy stability; Error estimates

1. Introduction

A mixed continuous–discontinuous Galerkin finite element model is constructed to solve several (geophysical) fluid equations in a generalized (potential) vorticity streamfunction formulation. Our algorithm

* Corresponding author. Tel.: +31 053 4893412; fax: +31 053 4894833.
E-mail addresses: E.Bernsen@phys.uu.nl (E. Bernsen), o.bokhove@math.utwente.nl (O. Bokhove), J.J.W.vanderVegt@math.utwente.nl (J.J.W. van der Vegt).

0021-9991/$ - see front matter © 2005 Elsevier Inc. All rights reserved.
doi:10.1016/j.jcp.2005.06.008

is an inviscid extension of the mixed continuous–discontinuous Galerkin finite element method presented in [9] for the incompressible two-dimensional Euler equations in a vorticity streamfunction formulation. We extend this method to the generalized formulation in a multiple connected domain with curved boundaries, and implement and test the algorithm more thoroughly. In particular, the circulation boundary condition around each connected part of the boundary or each "island" requires a modification, (17), of the usual function space for the continuous test and trial functions of the streamfunction.

The generalization consists of a hyperbolic equation for the (potential) vorticity, $\xi = \xi(x, y, t)$, and a linear elliptic equation for the streamfunction, $\psi = \psi(x, y, t)$, in a bounded domain $\Omega \subset \mathbb{R}^2$ as function of the horizontal coordinates x, y and time t. It is defined as follows:

$$\partial_t \xi / A + \nabla \cdot (\xi \vec{U}) = 0, \tag{1a}$$

$$\vec{U} = \nabla^{\perp} \psi, \tag{1b}$$

$$\nabla \cdot (A \nabla \psi) - B\psi + D = \xi / A \tag{1c}$$

with $0 < A_0 < A = A(x, y) < A_1 < \infty$ and $A_{0,1}$ strictly positive finite constants, $B = B(x,y) \geqslant 0$ and $D = D(x, y)$. The gradient operator is given by $\nabla = [\partial_x, \partial_y]^{\mathrm{T}}$ and the two-dimensional curl operator by $\nabla^{\perp} = [-\partial_y, \partial_x]^{\mathrm{T}}$. The system (1) is completed with boundary conditions and initial conditions in Section 3.

The generalized system (1) serves as a model for several fluid flow problems by choosing A, B and D to yield the incompressible two-dimensional (2D) Euler equations [7], the quasi-geostrophic equations [13], and the rigid-lid equations [8], often used in atmosphere and ocean dynamics. In all these cases ξ represents the (potential) vorticity of the fluid, $\vec{u} = A\vec{U}$ represents the velocity and $\vec{U}$ the (mass transport) velocity of the fluid. We explicitly consider the multiple connected and curved domains required in geophysical applications. This contrasts with [9], where the domain was simply connected and all numerical tests were done in rectangular domains. In these curved domains, it is essential to use isoparametric boundary elements, otherwise higher-order accuracy is impossible.

The outline of the paper is as follows. Details on the applications are provided in Section 2. In Section 4, we show that the energy and enstrophy of the generalized system (1) are conserved quantities, as well as Casimir invariants, for the slip flow boundary conditions introduced in Section 3. For the discretization of (1), we use the same method as in [9]. The equation for the vorticity, (1a), is discretized using a discontinuous Galerkin (DG) method, while for the elliptic equation, (1c), we use a continuous Galerkin discretization (see Section 5). In Section 6, we show that the spatial discretization of the generalized system leads to a scheme in which the energy and enstrophy are conserved and stable quantities. Moreover, discretizing time with an implicit θ- or modified midpoint-scheme, we also show energy and enstrophy to be conserved in time for $\theta = 1/2$. Numerical conservation of energy and enstrophy is essential for long-time stable integrations of geophysical systems (see, e.g. [10]). Further preservation of higher-order vortical integral constraints, in the form of numerical Casimir invariants, is also desirable, but not achieved here. Error estimates of the discretization are provided in Section 7. We verify the method and its implementation in Section 8, focusing on the convergence to several exact solutions as well as the properties of energy conservation and enstrophy stability. Finally, we summarize and conclude in Section 9.

2. Applications

The generalized vorticity streamfunction formulation given by (1) includes at least three distinct systems of interest.

(i) The 2D Euler equations [7] describe the flow of an incompressible fluid:

$$\partial_t \xi + \nabla \cdot (\vec{u} \xi) = 0, \tag{2a}$$

$$\vec{u} = \nabla^{\perp}\psi, \tag{2b}$$

$$\nabla^2\psi = \xi \tag{2c}$$

with $\xi = \partial_x v - \partial_y u$ the vertical component of the vorticity of the fluid, $\vec{u} = (u, v)^{\mathrm{T}}$ the velocity field and ψ the streamfunction. Defining $A = 1$, $B = D = 0$, and $\vec{U} = \vec{u}$, the Euler system (2) emerges as a special case of (1).

(ii) The quasi-geostrophic equations [13] approximately describe the motion of the atmosphere or oceans at mid-latitudes:

$$\partial_t \xi + \nabla \cdot (\vec{u}\xi) = 0, \tag{3a}$$

$$\vec{u} = \nabla^{\perp}\psi, \tag{3b}$$

$$\xi = \nabla^2\psi - \frac{f_0^2}{gD_0}\psi + \frac{f_0 h_{\mathrm{B}}}{D_0} + \beta y \tag{3c}$$

with the quasi-geostrophic potential vorticity ξ, D_0 a characteristic depth of the atmosphere or ocean, g the acceleration of gravity, the bottom topography at the vertical position $z = h_{\mathrm{B}} = h_{\mathrm{B}}(x,y)$, the Coriolis parameter $f_0 = 2\Omega_{\mathrm{e}} \sin\Theta_0$ and $\beta = 2\Omega_{\mathrm{e}} \cos\Theta_0/R$, where R is the radius of the Earth, Θ_0 a characteristic value of the latitude and Ω_{e} the Earth's rotation speed. Defining $A = 1$, $B = f_0^2/(gD_0)$, $D = f_0 h_{\mathrm{B}}/D_0 + \beta y$, and $\vec{U} = \vec{u}$, the quasi-geostrophic system (3) follows from (1).

(iii) The rigid-lid equations [8] describe the vertically averaged motion of fluid between topography at $z = h_{\mathrm{B}}(x,y)$ and a rigid lid at $z = h_{\mathrm{B}} + H$:

$$\partial_t \xi + \vec{u} \cdot \nabla\xi = 0, \tag{4a}$$

$$\vec{u} = (1/H)\nabla^{\perp}\psi, \tag{4b}$$

$$\xi = (\nabla^{\perp} \cdot \vec{u} + f)/H \tag{4c}$$

with ξ the potential vorticity, $\vec{u}$ the velocity field, f the Coriolis parameter and $0 < 1/A_1 < H = H(x,y) < 1/A_0 < \infty$ the depth of the fluid. Hence, by taking $A = 1/H$, $B = 0$, $D = f = f_0 + \beta y$ and $\vec{U} = H\vec{u}$, (4) emerges from (1).

3. Boundary and initial conditions

In [9] the domain was assumed to be simply connected which made it possible to consider one single Dirichlet boundary condition: $\psi|_{\partial\Omega} = 0$ with $\partial\Omega$ the boundary of Ω. In contrast, we focus on multiple connected curved domains with impenetrable walls, where, in general, we omit additional inflow and outflow boundary conditions for ease of presentation. This (part of the) boundary with slip flow boundary conditions is also denoted by $\partial\Omega_D$, on which

$$\vec{U} \cdot \hat{n} = 0 \tag{5}$$

holds with $\hat{n} = [n_x, n_y]^{\mathrm{T}}$ the outward unit vector normal to the boundary. The boundary $\partial\Omega_D$ is partitioned into N separate simply connected subsets. Thus, there exist $\partial\Omega_{D_i} \subset \partial\Omega_D$ such that

$$\cup_{i=1}^{N} \overline{\partial\Omega}_{D_i} = \overline{\partial\Omega}_D \quad \text{and} \quad \partial\Omega_{D_i} \cap \partial\Omega_{D_j} = \emptyset \tag{6}$$

for $i,j = 1,2,\ldots,N$ and $i \neq j$, where $\partial\Omega_{D_i} \cup \partial\Omega_{D_j}$ is not a simply connected set for $i \neq j$ (see Fig. 1).

On each part $\partial\Omega_{D_i}$ of the boundary, ψ is independent of x and y because $\partial\psi/\partial\hat{\tau} = \nabla\psi \cdot \hat{\tau} = -\nabla^{\perp}\psi \cdot \hat{n} \overset{(1b)}{=} -\vec{U} \cdot \hat{n} \overset{(5)}{=} 0$ with $\hat{\tau} = [-n_y, n_x]^{\mathrm{T}}$ the unit vector tangential to $\partial\Omega$. Hence, on these boundaries

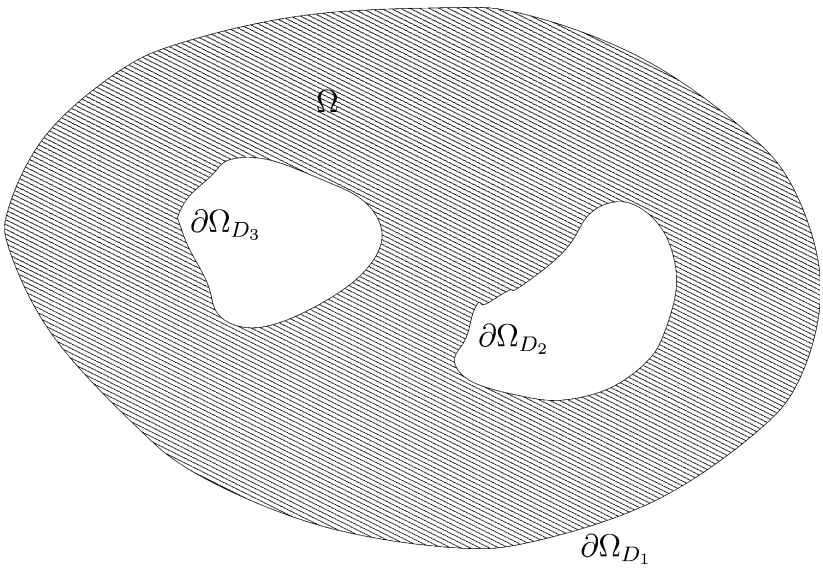

Fig. 1. An example of a domain, Ω, with slip flow boundary conditions. The boundary is partitioned into three separate parts: $\partial\Omega_{D_1}$, $\partial\Omega_{D_2}$ and $\partial\Omega_{D_3}$. Each of these three parts is a simply connected set.

$$\psi|_{\partial\Omega_{D_i}} = f_i(t) \tag{7}$$

is a function only depending on time. Consider the circulation $\mathscr{C}_i$ around $\partial\Omega_{D_i}$, defined by

$$\mathscr{C}_i = \int_{\partial\Omega_{D_i}} \vec{u}\cdot\hat{\tau}\,\mathrm{d}\Gamma = \int_{\partial\Omega_{D_i}} A\vec{U}\cdot\hat{\tau}\,\mathrm{d}\Gamma \tag{8}$$

with $\mathrm{d}\Gamma$ a line element along $\partial\Omega_D$. A relevant boundary condition at $\partial\Omega_{D_i}$, see [13], is

$$\mathrm{d}\mathscr{C}_i/\mathrm{d}t = 0, \tag{9}$$

whence the functions $f_i(t)$ in (7) are only implicitly defined.

Remark 1. Defining $f_i(t)$ using (9) for each $i = 1,2,\ldots,N$ defines ψ up to a constant. Therefore, for the case $B = 0$, we should prescribe $f_1(t) = 0$ on $\partial\Omega_{D_1}$ to enforce a unique solution ψ for (1c).

The initial conditions are specified by the vorticity field and the circulations $\mathscr{C}_i$ at $t = 0$. We calculate ψ (at $t = 0$) from (1c) using the boundary conditions. In Section 4, we show that the energy of the system (1) is a conserved quantity for the boundary conditions (5) and (9), provided that there are no parts of the boundary with inflow or outflow.

4. Conservation of energy and enstrophy

Energy and enstrophy are conserved quantities of the system (1) for the slip flow boundary conditions introduced in Section 3. Define the total energy $E(t)$ of the system (1) by

$$E(t) = \frac{1}{2}\|\sqrt{A}\nabla\psi\|_\Omega^2 + \frac{1}{2}\|\sqrt{B}\psi\|_\Omega^2, \tag{10}$$

where we require $A(x,y) > A_0 > 0$ and $B(x,y) \geqslant 0$. Here, the L^2-norm is denoted as $\|\cdot\|^2 = (\cdot,\cdot)$, while $(\cdot,\cdot)$ denotes the usual L^2-inner product with integration over the domain or sub domain, as indicated by a subscript.

Lemma 2. *The energy (10) of system (1) subject to slip flow boundary conditions, (5) and (9), is conserved*

$$\mathrm{d}E/\mathrm{d}t = 0. \tag{11}$$

Proof. Differentiating (1c) with respect to time and combining the result with (1a) gives $\nabla \cdot (A\nabla(\partial_t\psi)) - B\partial_t\psi = -\nabla \cdot (\vec{U}\xi)$. Multiplying this equation with ψ, integrating over the domain, and integrating by parts yields

$$-\frac{\mathrm{d}E}{\mathrm{d}t} = -\int_{\partial\Omega} A\psi\partial_t(\nabla\psi \cdot \hat{n})\,\mathrm{d}\Gamma + \int_{\Omega} \xi\vec{U} \cdot \nabla\psi\,\mathrm{d}\Omega - \int_{\partial\Omega} \xi\psi\vec{U} \cdot \hat{n}\,\mathrm{d}\Gamma. \tag{12}$$

The last two terms on the right-hand side of (12) vanish by using $\vec{U} \perp \nabla\psi$ and (5). The first term on the right-hand-side of (12) cancels as well since

$$\int_{\partial\Omega_D} A\psi\partial_t(\nabla\psi \cdot \hat{n})\,\mathrm{d}\Gamma \overset{(6)}{=} \sum_{i=1}^{N} \int_{\partial\Omega_{D_i}} A\psi\partial_t(\nabla\psi \cdot \hat{n})\,\mathrm{d}\Gamma \overset{(7)}{=} \sum_{i=1}^{N} f_i(t)\frac{\mathrm{d}}{\mathrm{d}t}\int_{\partial\Omega_{D_i}} A\nabla\psi \cdot \hat{n}\,\mathrm{d}\Gamma \overset{(8),(9)}{=} 0,$$

where we used the relation $\nabla\psi \cdot \hat{n} = \nabla^{\perp}\psi \cdot \hat{\tau}$. Hence, we find (11). □

The Casimirs invariants are

$$\mathscr{C}(t) = \int_{\Omega} (1/A)C_a(\xi)\,\mathrm{d}\Omega \tag{13}$$

with an arbitrary function $C_a = C_a(\xi)$ of the generalized vorticity. For the case $C_a(\xi) = \xi^2/2$, the enstrophy $S(t)$ emerges as a particularization

$$S(t) = \frac{1}{2}\|\xi/\sqrt{A}\|_{\Omega}^2. \tag{14}$$

Lemma 3. *The Casimirs (13) of system (1) , and thus the enstrophy (14), subject to the slip flow boundary condition, (5), are conserved*:

$$\mathrm{d}\mathscr{C}/\mathrm{d}t = 0 \quad \textit{and} \quad \mathrm{d}S/\mathrm{d}t = 0. \tag{15}$$

Proof. Result (15) emerges after we multiply (1a) by $C_a'(\xi) = \mathrm{d}C_a/\mathrm{d}\xi$ and use $\nabla \cdot (\vec{U}\xi) = \vec{U} \cdot \nabla\xi$ twice

$$(1/A)C_a'(\xi)\partial_t\xi + C_a'(\xi)\vec{U} \cdot \nabla\xi = (1/A)\partial_t C_a(\xi) + \nabla \cdot (\vec{U}C_a(\xi)) = 0, \tag{16}$$

integrate over the domain, Ω, and use the boundary conditions. □

5. Finite element method

We use a finite element method to solve the generalized vorticity equations (1). By discretizing the streamfunction with a continuous Galerkin finite element method in Section 5.1, we enforce continuity of the normal velocity through element boundaries. This simplifies the choice of the numerical flux in the DG discretization for (1a). In Section 5.3, we discuss time discretization schemes and, in Section 6,

the properties of the numerical method concerning the conservation and stability of energy and enstrophy of the numerical solution.[1]

5.1. Continuous Galerkin space discretization

Define the space of test functions $\mathsf{W}^1(\Omega)$ as follows:

$$\mathsf{W}^1(\Omega) = \{w \in H^1(\Omega) | \forall i \in \{1,2,\ldots,N\} \exists c_i \in \mathbb{R} : \|w - c_i\|_{\partial\Omega_{D_i}} = 0\} \tag{17}$$

with the standard $H^1(\Omega)$ Sobolev space and with $\|\cdot\|_{\partial\Omega_{D_i}}$ the $L^2(\partial\Omega_{D_i})$ norm. Note that $x \to \psi(x,t) \in \mathsf{W}^1(\Omega)$ with t fixed because of the boundary condition (7).

Remark 4. In the case $B = 0$, a Dirichlet boundary condition $\psi|_{\partial\Omega_1} = 0$ is used (see Remark 1), and instead of (17) we use

$$\mathsf{W}^1(\Omega) = \{w \in H^1(\Omega) | \|w\|_{\partial\Omega_{D_1}} = 0, \quad \forall i \in \{2,\ldots,N\} \exists c_i \in \mathbb{R} : \|w - c_i\|_{\partial\Omega_{D_i}} = 0\},$$

which ensures the weak formulation of (1c) to have a definite solution.

We multiply (1c) by a test function $w \in \mathsf{W}^1(\Omega)$ and integrate over the domain. For the first term this gives, after integrating by parts,

$$\int_\Omega \nabla \cdot (A\nabla\psi) w \,\mathrm{d}\Omega = \sum_{i=1}^{N} \int_{\partial\Omega_{D_i}} wA\nabla\psi \cdot \hat{n} \,\mathrm{d}\Gamma - \int_\Omega A\nabla\psi \cdot \nabla w \,\mathrm{d}\Omega.$$

Using (9) and the fact that $w \in \mathsf{W}^1(\Omega)$ is constant on each $\partial\Omega_{D_i}$, the boundary integral over $\partial\Omega_{D_i}$ $(i = 1,2,\ldots,N)$ yields

$$\int_{\partial\Omega_{D_i}} wA\nabla\psi \cdot \hat{n} \,\mathrm{d}\Gamma = \int_{\partial\Omega_{D_i}} wA\vec{U} \cdot \hat{\tau} \,\mathrm{d}\Gamma \overset{(17)}{=} w|_{\partial\Omega_{D_i}} \int_{\partial\Omega_{D_i}} A\vec{U} \cdot \hat{\tau} \,\mathrm{d}\Gamma \overset{(8)}{=} w|_{\partial\Omega_{D_i}} \mathscr{C}_i.$$

The weak formulation then becomes: Find $\psi \in \mathsf{W}^1(\Omega)$ such that for all $w \in \mathsf{W}^1(\Omega)$ the following holds:

$$L(\psi, w) = F_\xi(w) \tag{18}$$

with the operators L and F_ξ defined by:

$$L(v,w) = \left(\sqrt{A}\nabla v, \sqrt{A}\nabla w\right)_\Omega + \left(\sqrt{B}v, \sqrt{B}w\right)_\Omega, \tag{19}$$

$$F_\xi(w) = -(\xi/A, w)_\Omega + \int_\Omega Dw \,\mathrm{d}\Omega + \sum_{i=1}^{N} w|_{\partial\Omega_{D_i}} \mathscr{C}_i \tag{20}$$

for $v,w \in \mathsf{W}^1(\Omega)$. Note that L is a symmetric, coercive bilinear operator. Hence, $L(w,w) \geqslant \alpha\|w\|^2_{H^1(\Omega)}$ with $\alpha > 0$ $\forall w \in \mathsf{W}^1(\Omega)$, where coercivity is ensured in the case $B = 0$ by Remark 4. The proof of coercivity can be obtained by a minor change of the proof in Section 5.3 in [4]. Hence, the matrix of the system of linear equations in the finite element discretization is positive definite.

To approximate ψ and w in the discretized form of (18), we define the function space

$$\mathsf{W}^k_h = \mathsf{W}^1(\Omega) \cap X^k_h \tag{21}$$

[1] Additional technical appendices on the implementation are found in [3].

with X_h^k a finite element space consisting of continuous functions and including at least all polynomials of degree k on each element of a triangulation $\mathscr{T}_h = \{K\}$. We replace ψ, $w \in \mathsf{W}^1(\Omega)$ in (18) with the numerical approximations $\psi_h, w_h \in \mathsf{W}_h^k$ and approximate the vorticity with $\xi_h \in \mathsf{V}_h^k$ to be defined in Section 5.2. Hence, we obtain the discretized weak formulation: Find $\psi_h \in \mathsf{W}_h^k$ such that for each $w_h \in \mathsf{W}_h^k$ the following holds:

$$L(\psi_h, w_h) = F_{\xi_h}(w_h). \tag{22}$$

5.2. Discontinuous Galerkin space discretization

For the DG discretization, we define the space of discontinuous test functions

$$\mathsf{V}_h^k = \left\{ v_h | \forall K \in \mathscr{T}_h, \quad \exists w_h \in X_h^k : v_h|_K = w_h|_K \right\} \tag{23}$$

with $\mathscr{T}_h = \{K\}$ a triangulation of the domain and X_h^k the same continuous finite element space as in (21). We define V_h^k by (23), instead of

$$\tilde{\mathsf{V}}_h^k = \left\{ v_h | \forall K \in \mathscr{T}_h : v_h|_K \in \mathscr{P}_k(K) \right\} \tag{24}$$

with $\mathscr{P}_k(K)$ the usual space of polynomials on K of degree equal to or less than k, because conservation of energy of the numerical solution requires $\mathsf{W}_h^k \subset \mathsf{V}_h^k$ (see Section 6). The DG discretization is obtained by multiplying (1a) with a test function $v \in \mathsf{V}_h^k$ and integrating over $K \in \mathscr{T}_h$ to obtain

$$(\partial_t \xi / A, v)_K - (\xi \vec{U}, \nabla v)_K + (\xi U_n, v)_{\partial K} = 0 \tag{25}$$

with ∂K the boundary of an element $K \in \mathscr{T}_h$, and $U_n = \vec{U} \cdot \hat{n}$ the normal component of the velocity $\vec{U}$. Subsequently, we substitute the approximations $v_h, \xi_h \in \mathsf{V}_h^k$ into (25) with the approximate velocity field $\vec{U}_h = \nabla^\perp \psi_h$.

Define the inside, $v^- = \lim_{\epsilon \downarrow 0} v(\mathbf{x} + \epsilon \hat{n})$, and outside, $v^+ = \lim_{\epsilon \downarrow 0} v(\mathbf{x} + \epsilon \hat{n})$, trace values of a function v at a boundary point $\mathbf{x} = (x,y)^{\mathrm{T}}$ on ∂K. For the test function v_h on ∂K in (25), we choose the inside value v_h^-, while $\xi_h U_n$ on ∂K is replaced by a numerical flux $\hat{f}(\xi_h^+, \xi_h^-, U_n)$. Note that the normal transport velocity U_n is continuous across element boundaries because ψ_h is continuous and $U_n = \vec{U}_h \cdot \hat{n} = \nabla^\perp \psi_h \cdot \hat{n} = -\nabla \psi_h \cdot \hat{\tau} = -\mathrm{d}\psi_h / \mathrm{d}\hat{\tau}$. Hence, $\mathrm{d}\psi_h/\mathrm{d}\hat{\tau}$ and U_n are single valued on element boundaries. Only the vorticity ξ_h is multi valued.

The numerical flux satisfies the following properties:

(i) it is consistent

$$\hat{f}(\xi_h, \xi_h, U_n) = \xi_h U_n; \tag{26}$$

(ii) it is conservative

$$\hat{f}(\xi_h^+, \xi_h^-, U_n) = -\hat{f}(\xi_h^-, \xi_h^+, -U_n), \tag{27}$$

ensuring that the flux from two neighboring elements $K_L \in \mathscr{T}_h$ to $K_R \in \mathscr{T}_h$ is opposite to the flux from K_R to K_L; and

(iii) it is L^2-stable in the enstrophy norm (see Section 6), that is,

$$\left(\xi_h^+ - \xi_h^-\right) U_n (\hat{\xi}_h - \bar{\xi}_h) \leqslant 0 \tag{28}$$

with $\bar{\xi}_h = (\xi_h^+ + \xi_h^-)/2$ and $\hat{\xi}_h = \hat{f}(\xi_h^+, \xi_h^-, U_n)/U_n$. Hence, for $U_n > 0$ the value of the numerical flux is closer to the flux, $U_n \xi^-$, evaluated on the inside of the element than outside, $U_n \xi^+$.

The following fluxes $\hat{f}$ satisfy properties Eqs. (26)–(28):

$$\text{central} \quad \hat{f}(\xi^+, \xi^-, U_n) = \frac{\xi^+ + \xi^-}{2} U_n, \tag{29a}$$

$$\text{upwind} \quad \hat{f}(\xi^+, \xi^-, U_n) = U_n \begin{cases} \xi^+ & \text{if } U_n < 0, \\ \xi^- & \text{if } U_n \geqslant 0, \end{cases} \tag{29b}$$

$$\text{Lax–Friedrichs} \quad \hat{f}(\xi^+, \xi^-, U_n) = \frac{1}{2}(U_n(\xi^+ + \xi^-) - \alpha_{\mathrm{LF}}(\xi^+ - \xi^-)) \tag{29c}$$

with $\alpha_{\mathrm{LF}} \geqslant 0$. A common choice is $\alpha_{\mathrm{LF}} = \max|U_n|$ with a local or global maximum. For $\alpha_{\mathrm{LF}} = 0$ and $\alpha_{\mathrm{LF}} = |U_n|$, we obtain the central and upwind flux.

After replacing v_h with v_h^- and $\xi_h U_n$ with $\hat{f}(\xi_h^+, \xi_h^-, U_n)$ in (25), the weak formulation of (1a) is: find $\xi_h \in \mathsf{V}_h^k$ such that for all $v_h \in \mathsf{V}_h^k$ the following equation holds:

$$p_K(\partial_t \xi_h, v_h) = R_K(\xi_h, \psi_h, v_h) \tag{30}$$

with the operators p_K and R_K defined by:

$$p_K(u_h, v_h) = (u_h/A, v_h)_K, \tag{31}$$

$$R_K(u_h, w_h, v_h) = (u_h \nabla^\perp w_h, \nabla v_h)_K - \int_{\partial K} v_h^- \hat{f}(u_h^+, u_h^-, \nabla^\perp w_h \cdot \hat{n}) \, \mathrm{d}\Gamma \tag{32}$$

for $u_h, v_h \in \mathsf{V}_h^k$ and $w_h \in \mathsf{W}_h^k$. Note that we can formally write the space discretization as

$$\partial_t \xi_h = \mathscr{L}_h(\xi_h) \tag{33}$$

for an operator $\mathscr{L}_h$ following from (22) and (30).

5.3. Time discretization

5.3.1. Explicit scheme

For the test cases presented in Section 8, we use the explicit, third-order Runge–Kutta scheme (RK3) of [14] (see also [9]). The maximum size of the time step depends on the maximum velocity and the size of the elements. We performed a linear stability analysis for a space DG finite element and RK3 time discretization of the vorticity equation with constant velocity on a regular one-dimensional mesh, see Table 1.

5.3.2. Implicit scheme

Implicit methods usually have the advantage that the restriction on the time step is less severe, but at the expense of more computational cost per time step. We consider, inspired by the work in [17], the following θ- or modified midpoint-scheme [5] for the time discretization of (33):

Table 1
CFL-condition for different orders of basis functions for the discretized, linearized one-dimensional vorticity equation with constant velocity u

Basis functions	CFL (central flux)	CFL (upwind flux)
Constant	$\sqrt{3}$	1.25
Linear	$\sqrt{3}/4$	0.409
Quadratic	0.214	0.209
Cubic	0.130	0.130

The indicative time step for the RK3 time discretization in the nonlinear problem is then chosen such that $\Delta t \leqslant \mathrm{CFL}\, d_K/|\vec{u}_h|_{\max}$ with d_K the diameter of the inscribing circle of K and $\|\vec{u}_h\|_{\max} = \max_{\vec{x}\in K}\|A\vec{U}_h\|$ the maximum velocity in K.

$$\Delta\xi_h^n/\Delta t = \mathscr{L}_h(\xi_h^{n+\theta}) \tag{34}$$

with $\xi_h^{n+\theta} = \theta\xi_h^{n+1} + (1-\theta)\xi_h^n$ and $\Delta\xi_h^n = \xi_h^{n+1} - \xi_h^n$, for $\theta \in [0,1]$. Using (22) and (30), we find:

$$L(\psi_h^{n+\theta}, w_h) = F_{\xi_h^{n+\theta}}(w_h), \tag{35}$$

$$p_K(\Delta\xi_h^n, v_h) = \Delta t R_K(\xi_h^{n+\theta}, \psi_h^{n+\theta}, v_h), \tag{36}$$

for all $v_h \in \mathsf{V}_h^k$ and $w_h \in \mathsf{W}_h^k$. For each integer $n \geqslant 0$ and $w_h \in \mathsf{W}_h^k$, the streamfunction ψ_h^n is defined by

$$L(\psi_h^n, w_h) = F_{\xi_h^n}(w_h). \tag{37}$$

Note that (35) then is satisfied because

$$\psi_h^{n+\theta} = \theta\psi_h^{n+1} + (1-\theta)\psi_h^n, \tag{38}$$

and L and F are (bi-)linear operators.

6. Numerical conservation of energy and enstrophy

In Section 4, we showed that energy and enstrophy are conserved quantities for the slip flow boundary conditions described in Section 3. The energy and enstrophy of the discretization of (1) have similar properties.

Define the energy, E_h, of the numerical solution of (1)

$$E_h(t) = \frac{1}{2}\|\sqrt{A}\nabla\psi_h\|_\Omega^2 + \frac{1}{2}\|\sqrt{B}\psi_h\|_\Omega^2 = \frac{1}{2}L(\psi_h, \psi_h). \tag{39}$$

Theorems 6 and 7 are the counterparts of Lemma 2 for the numerical system. We use the following lemma.

Lemma 5. *Assume that we have slip flow boundary conditions, (5), then (32) satisfies*

$$\sum_{K\in\mathscr{T}_h} R_K(v_h, w_h, w_h) = 0 \tag{40}$$

for each $v_h \in \mathsf{V}_h^k$ and $w_h \in \mathsf{W}_h^k$.

Proof. Using definition (32) of R_K, we have

$$\sum_{K\in\mathscr{T}_h} R_K(v_h, w_h, w_h) = \sum_{K\in\mathscr{T}_h}\int_K v_h\nabla^\perp w_h\cdot\nabla w_h\,\mathrm{d}K - \sum_{K\in\mathscr{T}_h}\int_{\partial K} w_h^-\hat{f}(v_h^+, v_h^-, \nabla^\perp w_h\cdot\hat{n})\,\mathrm{d}\Gamma,$$

where the interior integral vanishes because $\nabla^\perp w_h \perp \nabla w_h$. The summation over the element boundary integrals vanishes because w_h is continuous across element boundaries ($w_h^+ = w_h^-$), the conservation property of the numerical flux (27), and the slip flow boundary conditions. □

Theorem 6. *Consider the solution of (22) and (30) subject to slip flow boundary conditions, (5). The energy associated with this numerical solution, as given by (39), is a conserved quantity*

$$\mathrm{d}E_h/\mathrm{d}t = 0. \tag{41}$$

Proof. We prove that (41) holds at each point in time. First choose an arbitrary, but fixed, point in time, denoted by t_0. Differentiate (22) with respect to time and use (30) to obtain for all $w_h \in \mathsf{W}_h^k$ at $t = t_0$

$$[L(\partial_t\psi_h, w_h)]_{t=t_0} = -\sum_{K\in\mathscr{T}_h} p_K([\partial_t\xi_h]_{t=t_0}, w_h) \overset{(30)}{=} -\sum_{K\in\mathscr{T}_h} R_K([\xi_h]_{t=t_0}, [\psi_h]_{t=t_0}, w_h).$$

Now choose $w_h = [\psi_h]_{t=t_0}$ and apply Lemma 5 to obtain

$$\left[\frac{\mathrm{d}E_h}{\mathrm{d}t}\right]_{t=t_0} = L([\partial_t\psi_h]_{t=t_0}, [\psi_h]_{t=t_0}) = -\sum_{K\in\mathscr{T}_h} R_K([\xi_h]_{t=t_0}, [\psi_h]_{t=t_0}, [\psi_h]_{t=t_0}) = 0.$$

Since t_0 was chosen arbitrary, we find (41). □

Note that an essential step consists of using $w_h = \psi_h$ as a test function in the DG discretization (30). The space of test functions for the continuous Galerkin discretization must, therefore, satisfy $\mathsf{W}_h^k \subset \mathsf{V}_h^k$.

Denote the numerical energy at time level n by $E_h^n = L(\psi_h^n, \psi_h^n)/2$. The implicit time discretization scheme has the property that for certain choices of θ the numerical energy is conserved.

Theorem 7. *Consider the solution of (36) and (35) subject to slip flow boundary conditions, (5) and (9). For $\theta \in [\frac{1}{2}, 1]$, the numerical energy is stable*

$$\Delta E_h^n \equiv E_h^{n+1} - E_h^n \leqslant 0. \tag{42}$$

For $\theta = \frac{1}{2}$, the numerical energy is conserved

$$\Delta E_h^n = 0. \tag{43}$$

Proof. We combine (37) to obtain for each $w_h \in \mathsf{W}_h^k$

$$L(\Delta\psi_h^n, w_h) = F_{\xi_h^{n+1}}(w_h) - F_{\xi_h^n}(w_h)$$

with $\Delta\psi_h^n = \psi_h^{n+1} - \psi_h^n$. Since $w_h \in \mathsf{W}_h^k \subset \mathsf{V}_h^k$, we use (20), (31), (36) and $\Delta\xi_h^n = \xi_h^{n+1} - \xi_h^n$ to write

$$F_{\xi_h^{n+1}}(w_h) - F_{\xi_h^n}(w_h) = -\sum_{K\in\mathscr{T}_h} p_K(\Delta\xi_h^n, w_h) \overset{(36)}{=} -\sum_{K\in\mathscr{T}_h} \Delta t R_K(\xi_h^{n+\theta}, \psi_h^{n+\theta}, w_h).$$

Combining the above two equations, choosing $w_h = \psi_h^{n+\theta}$ and applying Lemma 5 gives

$$L(\Delta\psi_h^n, \psi_h^{n+\theta}) = -\sum_{K\in\mathscr{T}_h} \Delta t R_K(\xi_h^{n+\theta}, \psi_h^{n+\theta}, \psi_h^{n+\theta}) = 0.$$

As the operator L is bilinear and symmetric, we use (38) to obtain (see [17])

$$\Delta E_h^n = L(\Delta\psi_h^n, \psi_h^{n+\theta}) - \left(\theta - \frac{1}{2}\right) L(\Delta\psi_h^n, \Delta\psi_h^n).$$

Thus, we find

$$\Delta E_h^n = -\left(\theta - \frac{1}{2}\right) L(\Delta\psi_h^n, \Delta\psi_h^n).$$

Since $L(w_h, w_h) \geqslant 0$ for each $w_h \in \mathsf{W}_h^k$ and $\psi_h \in \mathsf{W}_h^k$, we obtain $\Delta E_h^n \leqslant 0$ for $\theta \in [\frac{1}{2}, 1]$ and $\Delta E_h^n = 0$ for $\theta = \frac{1}{2}$. □

Define the numerical enstrophy S_h

$$S_h(t) = \frac{1}{2}\|\xi_h/\sqrt{A}\|^2. \tag{44}$$

Theorems 9 and 10 are the counterparts of Lemma 3 for the numerical system. We use the following lemma.

Lemma 8. *Assume that we have slip flow boundary conditions (5). For each $v_h \in \mathsf{V}_h^k$ and $w_h \in \mathsf{W}_h^k$, the operator R_K defined in (32) satisfies*

$$\sum_{K\in\mathscr{T}_h} R_K(v_h, w_h, v_h) \leqslant 0. \tag{45}$$

For the central flux (29a), one has

$$\sum_{K\in\mathscr{T}_h} R_K(v_h, w_h, v_h) = 0. \tag{46}$$

Proof. Using definition (32) of R_K we have

$$\sum_{K\in\mathscr{T}_h} R_K(v_h, w_h, v_h) = \sum_{K\in\mathscr{T}_h} \int_K v_h \nabla^\perp w_h \cdot \nabla v_h \,\mathrm{d}K - \sum_{K\in\mathscr{T}_h} \int_{\partial K} v_h^- \hat{f}(v_h^+, v_h^-, U_n)\,\mathrm{d}\Gamma \tag{47}$$

with $U_n = \nabla^\perp w_h \cdot \hat{n}$. After integration by parts and using the boundary conditions, (47) becomes

$$\begin{aligned}\sum_{K\in\mathscr{T}_h} R_K(v_h, w_h, v_h) &= \sum_{K\in\mathscr{T}_h} \int_{\partial K} U_n \left(\frac{1}{2}(v_h^-)^2 - v_h^- \hat{v}_h\right) \mathrm{d}\Gamma \\ &= \sum_{K\in\mathscr{T}_h} \int_{\partial K} \frac{1}{2} U_n [v_h](\hat{v}_h - \overline{v}_h)\,\mathrm{d}\Gamma + \sum_{K\in\mathscr{T}_h} \int_{\partial K} U_n \left(\frac{1}{2}\overline{v_h^2} - \overline{v}_h \hat{v}_h\right) \mathrm{d}\Gamma \end{aligned} \tag{48}$$

with $\overline{v}_h = (v_h^+ + v_h^-)/2$, $\overline{v_h^2} = ((v_h^+)^2 + (v_h^-)^2)/2$, $[v_h] = v_h^+ - v_h^-$ and $\hat{v}_h = \hat{f}(v_h^+, v_h^-, U_n)/U_n$. The second summation in (48) vanishes because of (27) and the boundary condition $\vec{U}\cdot\hat{n} = 0$. The first term in (48) is smaller than or equal to zero because of (28). Hence, (45) emerges. For the central flux (29a) by using the equality in (28), the first term in (48) also vanishes. Hence, we obtain (46). □

The following theorem shows that the enstrophy of the numerical solution of (1) is conserved or stable. Note that time is not yet discretized.

Theorem 9. *Consider the solution of (22) and (30) subject to slip flow boundary conditions (5). The enstrophy associated with this numerical solution, as given by (44), is a stable quantity*

$$\mathrm{d}S_h/\mathrm{d}t \leqslant 0. \tag{49}$$

For the central flux (29a), (49) becomes an equality.

Proof. We rewrite

$$\mathrm{d}S_h/\mathrm{d}t = \sum_{K\in\mathscr{T}_h} p_K(\partial_t \xi_h, \xi_h). \tag{50}$$

Using (30) with $v_h = \xi_h$ and Lemma 8, we obtain

$$\sum_{K\in\mathscr{T}_h} p_K(\partial_t \xi_h, \xi_h) = \sum_{K\in\mathscr{T}_h} R_K(\xi_h, \psi_h, \xi_h) \leqslant 0. \tag{51}$$

Combining (50) and (51) yields (49). Using the central flux and Lemma 8, the equality in (49) is obtained. □

Denote the numerical enstrophy at time level n by S_h^n. Using the θ-scheme, the numerical enstrophy is stable for certain choices of θ.

Theorem 10. *Consider the solution of (35) and (36) subject to slip flow boundary conditions (5). For $\theta \in [\frac{1}{2}, 1]$, the numerical enstrophy is stable*

$$\Delta S_h^n \equiv S_h^{n+1} - S_h^n \leqslant 0. \tag{52}$$

For the central flux (29a) with $\theta = \frac{1}{2}$ the enstrophy is conserved

$$\Delta S_h^n = 0. \tag{53}$$

Proof. Take $v_h = \xi_h^{n+\theta}$ in (36) to obtain

$$\sum_{K\in\mathcal{T}_h} p_K(\Delta\xi_h^n, \xi_h^{n+\theta}) = \sum_{K\in\mathcal{T}_h} R_K(\xi_h^{n+\theta}, \psi_h^{n+\theta}, \xi_h^{n+\theta}). \tag{54}$$

Because the operator p_K is bilinear and symmetric, we find after using (54):

$$\Delta S_h^n = \sum_{K\in\mathcal{T}_h} p_K(\Delta\xi_h^n, \xi_h^{n+\theta}) - \left(\theta - \frac{1}{2}\right) \sum_{K\in\mathcal{T}_h} p_K(\Delta\xi_h^n, \Delta\xi_h^n) \tag{55}$$

$$= \sum_{K\in\mathcal{T}_h} R_K(\xi_h^{n+\theta}, \psi_h^{n+\theta}, \xi_h^{n+\theta}) - \left(\theta - \frac{1}{2}\right) \sum_{K\in\mathcal{T}_h} p_K(\Delta\xi_h^n, \Delta\xi_h^n). \tag{56}$$

If we choose $\theta \in [\frac{1}{2}, 1]$, then we find (52) because of Lemma 8 and $p_K(v_h,v_h) \geqslant 0$ for each $v_h \in \mathsf{V}_h^k$. If we choose $\theta = \frac{1}{2}$, then the second term of (56) vanishes. If, additionally, the central flux (29a) is used, then the first term vanishes as well because of Lemma 8. Hence, we obtain (53). □

7. Error estimates

In this section, we will state error estimates for the numerical discretization discussed in this paper. The error analysis for the Euler equations presented in [9] has been extended to the numerical scheme given by (22) and (30). The main differences with the analysis in [9] concern the elliptic part of the problem and the fact that we make the dependence of the error on the (generalized) vorticity explicit. In addition, we impose a slightly less restrictive condition on the vorticity field than in [9], where the condition $\xi \in H^{k+1}(\Omega)$, with $k > 1$, is required. An error estimate which imposes minimal smoothness requirements on the (generalized) vorticity field will be published elsewhere since this rather technical analysis is outside the scope of this paper [16].

We now state the main error estimate:

Theorem 11. *Assume that Ω is a bounded domain with Lipschitz boundary $\partial\Omega$. In addition, we assume that the coefficients in (1c) satisfy $A, B \in C^{1,1}(\overline{\Omega})$, $D \in L^\infty(\Omega)$, with*

$$A_0 = \operatorname{ess\,inf}\{A(x,y) | (x,y) \in \Omega\} > 0, \quad B_0 = \operatorname{ess\,inf}\{B(x,y) | (x,y) \in \Omega\} \geqslant 0,$$

and that the vorticity field ξ belongs to $L^2([0,T], W^1_\infty(\Omega) \cap H^{k+1}(\Omega))$, with $k \geqslant 1$. Then the error in the DG finite element discretization (22) and (30), with the numerical flux given by one of (29a)–(29c), subject to the slip flow boundary condition (5), on a quasi-uniform mesh $\mathcal{T}_h$ with sufficiently small mesh size $h \leqslant h_0 \leqslant 1$, can be estimated as

$$\|\vec{u} - \vec{u}_h\|_{L^2(\Omega)} + \|\xi - \xi_h\|_{L^2(\Omega)} \leqslant Ch^k \exp\left(CT \sup_{t\in[0,T]} (\|\nabla\xi(\cdot,t)\|_{L^\infty(\Omega)}, \|\xi(\cdot,t)\|_{H^{k+1}(\Omega)})\right)$$
$$\times \left(\|\xi(\cdot,0)\|^2_{H^k(\Omega)} + \int_0^T \|\xi(\cdot,t)\|^2_{H^{k+1}(\Omega)}\,\mathrm{d}t\right)^{\frac{1}{2}},$$

with k the order of the polynomial basis functions in the DG discretization and C a positive constant, independent of h, ξ and $\vec{u}$.

Corollary 12. *The L^∞-norm of the error in the velocity field can be estimated as*

$$\|\vec{u}-\vec{u}_h\|_{L^\infty(\Omega)} \leqslant Ch^k \sup_{t\in[0,T]} \|\xi(\cdot,t)\|_{H^k(\Omega)} + Ch^{-1}\|\vec{u}-\vec{u}_h\|_{L^2(\Omega)}.$$

Remark 13. An upper bound for the minimum mesh size h_0 is

$$h_0 = \min\left(\frac{\sqrt{A_0}}{C_I C_R C_{AB}\sqrt{4(2b+1)}}, 1\right),$$

with $b \geqslant \frac{1}{2}A_0 - B_0$, C_R the regularity constant for the differential operator (1c) on the Lipschitz domain Ω, C_I the constant in the interpolation estimate for the projection from $H^2(\Omega)$ onto W_h^k and $C_{AB} = \max(\|A\|_{L^\infty(\Omega)}, \|B\|_{L^\infty(\Omega)})$.

Remark 14. If $B_0 \geqslant \frac{1}{2}A_0 + \frac{1}{2}$ then there is no restriction on the mesh size h_0 and $h \leqslant 1$ is a sufficient condition for Theorem 11.

Here $H^k(\Omega)$ denotes the Hilbert space of k-times weakly differentiable functions which are square integrable, including all derivatives up to the order k, $L^\infty(\Omega)$ is the space of essentially bounded functions, $W^1_\infty(\Omega)$ the space of essentially bounded functions with also a bounded weak derivative, and $C^{1,1}(\overline{\Omega})$ the space of Hölder continuous functions.

For a detailed proof and the definition of the function spaces and norms we refer to Appendix B.

8. Verification

In this section, we present some examples which test the numerical method. We implemented the finite element method described using the C++ programming language. Each of the applications discussed in Section 2 is tested with the Runge–Kutta time discretization discussed in Section 5.3.1 for the central flux (29a) as well as the upwind flux (29b).

8.1. Example 1: Stuart vortex

First, we consider the Stuart vortex, which is a stationary solution for the 2D Euler equations (see Section 2 and Appendix A.1). The coarsest mesh $\mathscr{T}_1$ used in the simulations is shown in Fig. 2. The upper and lower boundary and the boundary of the island in the center of the domain coincide with streamlines of the exact solution. The left and right boundaries are periodic. On the upper and lower boundaries we prescribe a value of the streamfunction given by

$$\mathscr{C}_{low} = \mathscr{C}_{up} = \int_{\partial\Omega_{up}} A\vec{U}\cdot\hat{\tau}\,d\Gamma \approx 6.180637249. \tag{57}$$

On the boundary of the island in the center of the domain we impose the exact value of the streamfunction (see Remark 1).

We tested our implementation up to cubic basis functions, and used an unstructured quadrilateral basic grid. To obtain the orders of convergence for the L^1-, L^2- and L^∞-errors, given in Tables 2–5, this basic grid was refined in a structured manner up to three times. For internal elements this grid refinement is straightforward, while for boundary elements the curvature of the boundary was taken into account. Note that vorticity and streamfunction converge as $O(h^{k+1})$ in the upwind case for the L^1- and L^2-errors, one order higher than the error estimates. Here and in the remaining tests, the absolute value of the error is larger for

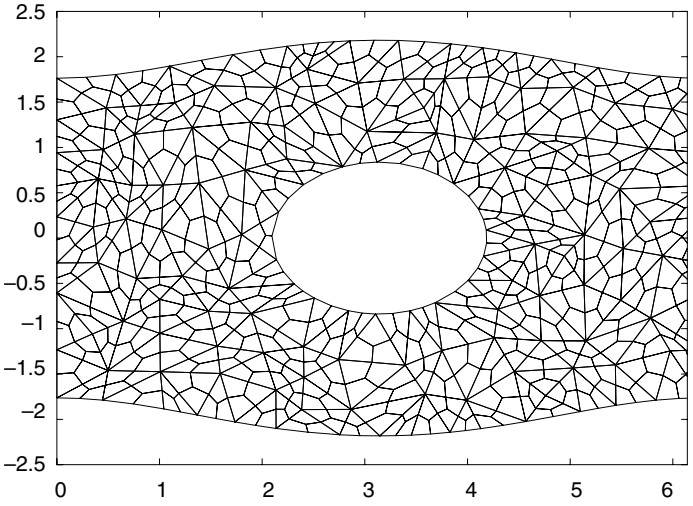

Fig. 2. The coarsest mesh $\mathscr{T}_1$ with 720 elements.

Table 2
Errors in ξ_h for the Stuart vortex at $t = 8$ using the upwind flux

k	$\mathscr{T}_h$	L_1-error	Order	L_2-error	Order	L_∞-error	Order
1	720	1.94e − 01	–	8.22e − 02	–	1.22e − 01	–
	2880	5.80e − 02	1.74	3.21e − 02	1.35	6.15e − 02	0.99
	11,520	1.52e − 02	1.94	1.05e − 02	1.61	2.60e − 02	1.24
	46,080	3.32e − 03	2.19	2.68e − 03	1.97	8.91e − 03	1.55
2	720	1.47e − 02	–	7.20e − 03	–	1.61e − 02	–
	2880	1.57e − 03	3.23	9.86e − 04	2.87	2.95e − 03	2.44
	11,520	1.51e − 04	3.38	1.24e − 04	2.99	5.00e − 04	2.56
	46,080	1.26e − 05	3.58	1.33e − 05	3.22	7.54e − 05	2.73
3	720	1.48e − 02	–	7.53e − 03	–	1.69e − 02	–
	2880	8.26e − 04	4.17	5.60e − 04	3.75	1.97e − 03	3.10
	11,520	4.39e − 05	4.23	3.25e − 05	4.11	1.82e − 04	3.44
	46,080	2.29e − 06	4.26	1.76e − 06	4.21	1.45e − 05	3.65

The L^1-, L^2- and L^∞-errors and orders of convergence for kth-order basis functions with $k = 1, 2, 3$ are shown.

the central flux and the convergence is slower than for the upwind flux, but is in accordance with our error estimates. It means that the polynomial order k should be larger than one. The order of convergence for the L^∞-error is also lower in all tests. Numerical results are shown in Fig. 3 for the vorticity and streamfunction at time $t = 8$. The use of isoparametric elements at the curved boundaries is essential to reach convergence for $k \geqslant 2$. When the curvature at the boundary is approximated with low-order (piecewise linear) elements at the boundary, the inversion required to obtain ψ from the elliptic equation transports the local lack of accuracy instantly into the entire domain.

8.2. Example 2: A traveling wave solution

Consider a traveling wave solution for the quasi-geostrophic equations on a β-plane (see Section 2 and Appendix A.2). The domain is $\Omega = [0, 2\pi]^2$ with periodic boundary conditions on the left and right

Table 3
Errors in ξ_h for the Stuart vortex at $t = 8$ using the central flux

k	$\mathscr{T}_h$	L_1-error	Order	L_2-error	Order	L_∞-error	Order
1	720	5.83e − 01	–	1.78e − 01	–	4.04e − 01	–
	2880	3.44e − 01	0.76	1.06e − 01	0.75	2.18e − 01	0.89
	11,520	2.18e − 01	0.66	6.67e − 02	0.66	2.03e − 01	0.10
	46,080	1.24e − 01	0.81	3.82e − 02	0.80	1.02e − 01	0.99
2	720	1.54e − 01	–	4.93e − 02	–	9.45e − 02	–
	2880	1.35e − 02	3.51	4.75e − 03	3.38	1.66e − 02	2.51
	11,520	1.85e − 03	2.87	6.35e − 04	2.90	1.86e − 03	3.16
	46,080	2.36e − 04	2.97	7.98e − 05	2.99	3.44e − 04	2.43
3	720	6.34e − 02	–	1.95e − 02	–	4.28e − 02	–
	2880	8.03e − 03	2.98	2.56e − 03	2.93	6.99e − 03	2.61
	11,520	9.21e − 04	3.12	3.11e − 04	3.04	1.30e − 03	2.43
	46,080	1.13e − 04	3.02	3.89e − 05	3.00	1.91e − 04	2.76

The L^1-, L^2- and L^∞-errors and orders of convergence for kth-order basis functions are shown.

Table 4
Errors in ψ_h for the Stuart vortex at $t = 8$ using the upwind flux

k	$\mathscr{T}_h$	L_1-error	Order	L_2-error	Order	L_∞-error	Order
1	720	8.13e − 02	–	1.90e − 02	–	1.26e − 02	–
	2880	1.78e − 02	2.19	4.20e − 03	2.18	3.50e − 03	1.85
	11,520	4.22e − 03	2.08	1.00e − 03	2.06	9.58e − 04	1.87
	46,080	1.02e − 03	2.05	2.44e − 04	2.04	2.69e − 04	1.83
2	720	4.99e − 03	–	1.15e − 03	–	8.61e − 04	–
	2880	3.53e − 04	3.82	8.10e − 05	3.83	9.48e − 05	3.18
	11,520	2.42e − 05	3.87	5.97e − 06	3.76	1.64e − 05	2.53
	46,080	1.93e − 06	3.65	5.51e − 07	3.44	2.45e − 06	2.75
3	720	4.39e − 03	–	1.02e − 03	–	7.41e − 04	–
	2880	3.12e − 04	3.81	6.96e − 05	3.88	5.34e − 05	3.79
	11,520	1.92e − 05	4.02	4.25e − 06	4.03	3.86e − 06	3.79
	46,080	1.26e − 06	3.94	2.77e − 07	3.94	2.96e − 07	3.71

The L^1-, L^2- and L^∞-errors and orders of convergence for kth-order basis functions are shown.

Table 5
Errors in ψ_h for the Stuart vortex at $t = 8$ using the central flux

k	$\mathscr{T}_h$	L_1-error	Order	L_2-error	Order	L_∞-error	Order
1	720	9.68e − 02	–	2.27e − 02	–	1.26e − 02	–
	2880	2.40e − 02	2.01	5.70e − 03	1.99	3.73e − 03	1.76
	11,520	5.94e − 03	2.02	1.47e − 03	1.96	1.18e − 03	1.66
	46,080	1.61e − 03	1.89	3.83e − 04	1.94	3.65e − 04	1.69
2	720	6.04e − 03	–	1.51e − 03	–	1.02e − 03	–
	2880	3.58e − 04	4.08	8.32e − 05	4.18	9.39e − 05	3.44
	11,520	2.40e − 05	3.90	5.98e − 06	3.80	1.64e − 05	2.51
	46,080	1.93e − 06	3.63	5.52e − 07	3.44	2.45e − 06	2.74
3	720	4.35e − 03	–	1.04e − 03	–	7.90e − 04	–
	2880	3.04e − 04	3.84	6.84e − 05	3.92	5.48e − 05	3.85
	11,520	1.91e − 05	3.99	4.24e − 06	4.01	3.85e − 06	3.83
	46,080	1.26e − 06	3.92	2.78e − 07	3.93	2.96e − 07	3.70

The L^1-, L^2- and L^∞-errors and orders of convergence for kth-order basis functions are shown.

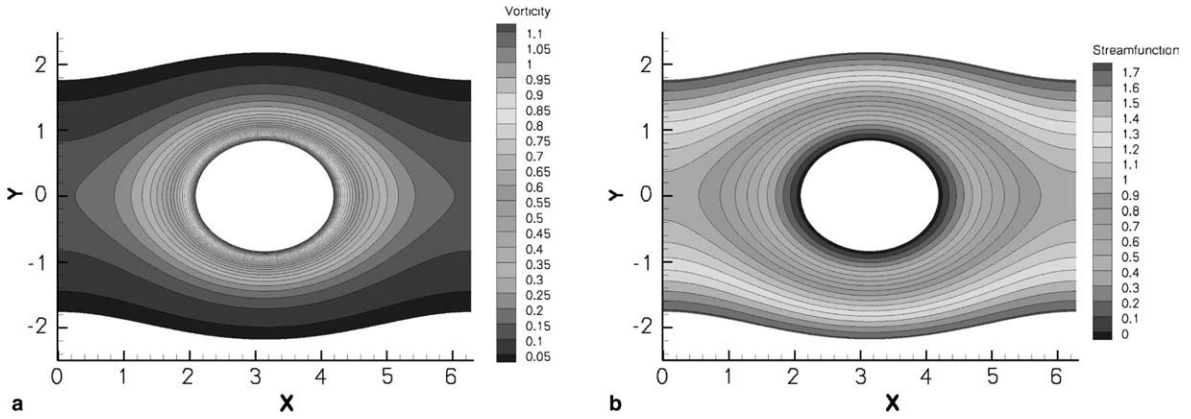

Fig. 3. The (a) vorticity and (b) streamfunction field at $t = 8$ for the Stuart vortex.

boundary. On the upper and lower boundaries we prescribe the circulation of the exact solution as $\mathscr{C}_{\text{low}} = \mathscr{C}_{\text{up}} = 0$. The solutions are seen to converge to $O(h^{k+1})$ for the vorticity and streamfunction in Tables 6 and 8 for the L^1- and L^2-errors using the upwind flux, and to $O(h^k)$ in Tables 7 and 9 for the central flux. For $k = 1$, we seem to have a slow convergence in L^∞ for the central flux, which may hint at an inconsistency. Numerical results are shown in Fig. 4.

Theorems 6 and 9 state that the energy and enstrophy of the numerical discretization in space are conserved and stable for a spatial discretization only. To illustrate these theorems using a Runge–Kutta time discretization, it is, therefore, necessary to refine the time step. Consider the numerical solution on a 32×32 grid using various time steps for quadratic basis functions. Figs. 5 and 6 show the relative change in energy and enstrophy of the numerical solution for different time steps for the upwind flux as well as the central flux. In Fig. 5, the energy of the numerical solution appears to converge to a constant value for a decreasing time step. Fig. 6(a) illustrates similar convergence for the enstrophy when using a central flux. However, for an upwind flux, the enstrophy is only a stable but not a conserved quantity, as follows from Fig. 6(b). These results are consistent with Theorems 6 and 9. It is also verified from these results that RK3 is third-order in time.

Table 6
Errors in ξ_h for the traveling wave example at $t = 12\pi$ using the upwind flux

k	$\mathscr{T}_h$	L_1-error	Order	L_2-error	Order	L_∞-error	Order
1	8×8	1.27e + 01	–	2.50e + 00	–	9.57e − 01	–
	16×16	3.18e + 00	1.99	6.15e − 01	2.02	2.35e − 01	2.03
	32×32	7.41e − 01	2.10	1.44e − 01	2.09	5.48e − 02	2.10
	64×64	1.77e − 01	2.07	3.47e − 02	2.05	1.54e − 02	1.83
2	8×8	8.67e − 01	–	1.76e − 01	–	8.04e − 02	–
	16×16	7.93e − 02	3.45	1.72e − 02	3.35	1.25e − 02	2.68
	32×32	1.28e − 02	2.63	3.31e − 03	2.38	2.82e − 03	2.15
	64×64	1.86e − 03	2.79	6.25e − 04	2.41	8.69e − 04	1.70
3	8×8	5.02e − 02	–	1.16e − 02	–	1.24e − 02	–
	16×16	2.00e − 03	4.65	5.28e − 04	4.45	8.14e − 04	3.93
	32×32	1.09e − 04	4.19	2.95e − 05	4.16	9.22e − 05	3.14
	64×64	6.90e − 06	3.98	1. 81e − 06	4.02	9.49e − 06	3.28

The L^1-, L^2- and L^∞-errors and orders of convergence for kth-order basis functions are shown.

Table 7
Errors in ξ_h for the traveling wave example at $t = 12\pi$ using the central flux

k	$\mathcal{T}_h$	L_1-error	Order	L_2-error	Order	L_∞-error	Order
1	8×8	3.07e + 01	–	5.95e + 00	–	2.93e + 00	–
	16×16	1.16e + 01	1.41	2.39e + 00	1.32	1.51e + 00	0.96
	32×32	6.65e + 00	0.80	1.43e + 00	0.74	1.55e + 00	−0.04
	64×64	9.03e − 01	2.88	2.06e − 01	2.79	2.70e − 01	2.52
2	8×8	1.41e + 00	–	2.99e − 01	–	2.26e − 01	–
	16×16	1.93e − 01	2.87	4.06e − 02	2.88	3.50e − 02	2.69
	32×32	2.97e − 02	2.71	6.18e − 03	2.71	5.10e − 03	2.78
	64×64	6.36e − 03	2.22	1.34e − 03	2.20	1.55e − 03	1.72
3	8×8	3.35e − 01	–	7.13e − 02	–	6.98e − 02	–
	16×16	3.09e − 02	3.44	6.54e − 03	3.45	7.36e − 03	3.25
	32×32	4.37e − 03	2.82	9.35e − 04	2.81	1.15e − 03	2.68
	64×64	3.20e − 04	3.77	6.84e − 05	3.77	9.72e − 05	3.57

The L^1-, L^2- and L^∞-errors and orders of convergence for kth-order basis functions are shown.

Table 8
Errors in ψ_h for the traveling wave at $t = 12\pi$ using the upwind flux

k	$\mathcal{T}_h$	L_1-error	Order	L_2-error	Order	L_∞-error	Order
1	8×8	4.31e + 00	–	8.31e − 01	–	2.67e − 01	–
	16×16	1.06e + 00	2.03	2.04e − 01	2.03	6.47e − 02	2.05
	32×32	2.45e − 01	2.11	4.75e − 02	2.10	1.53e − 02	2.08
	64×64	5.80e − 02	2.08	1.13e − 02	2.07	3.66e − 03	2.06
2	8×8	1.00e − 01	–	1.98e − 02	–	9.10e − 03	–
	16×16	9.23e − 03	3.44	1.77e − 03	3.49	7.11e − 04	3.68
	32×32	1.09e − 03	3.08	1.96e − 04	3.18	6.99e − 05	3.35
	64×64	1.36e − 04	3.00	2.43e − 05	3.01	8.18e − 06	3.10
3	8×8	1.04e − 02	–	2.28e − 03	–	1.26e − 03	–
	16×16	4.53e − 04	4.52	1.14e − 04	4.33	7.59e − 05	4.06
	32×32	2.70e − 05	4.07	6.91e − 06	4.04	4.72e − 06	4.01
	64×64	1.67e − 06	4.02	4.29e − 07	4.01	2.92e − 07	4.01

The L^1-, L^2- and L^∞-errors and orders of convergence for kth-order basis functions are shown.

Table 9
Errors in ψ_h for the traveling wave at $t = 12\pi$ using the central flux

k	$\mathcal{T}_h$	L_1-error	Order	L_2-error	Order	L_∞-error	Order
1	8×8	8.72e + 00	–	1.63e + 00	–	5.05e − 01	–
	16×16	2.76e + 00	1.66	5.21e − 01	1.64	1.70e − 01	1.57
	32×32	1.09e + 00	1.34	2.05e − 01	1.35	6.89e − 02	1.30
	64×64	5.32e − 02	4.36	1.01e − 02	4.34	3.25e − 03	4.41
2	8×8	1.27e − 01	–	2.59e − 02	–	1.16e − 02	–
	16×16	8.80e − 03	3.85	1.65e − 03	3.97	7.05e − 04	4.04
	32×32	1.10e − 03	3.00	2.03e − 04	3.03	8.05e − 05	3.13
	64×64	1.37e − 04	3.00	2.50e − 05	3.02	8.22e − 06	3.29
3	8×8	1.15e − 02	–	2.44e − 03	–	1.44e − 03	–
	16×16	2.13e − 03	2.43	4.19e − 04	2.54	1.53e − 04	3.23
	32×32	8.90e − 05	4.58	1.77e − 05	4.57	7.50e − 06	4.35
	64×64	2.30e − 06	5.27	5.03e − 07	5.13	3.07e − 07	4.61

The L^1-, L^2- and L^∞-errors and orders of convergence for kth-order basis functions are shown.

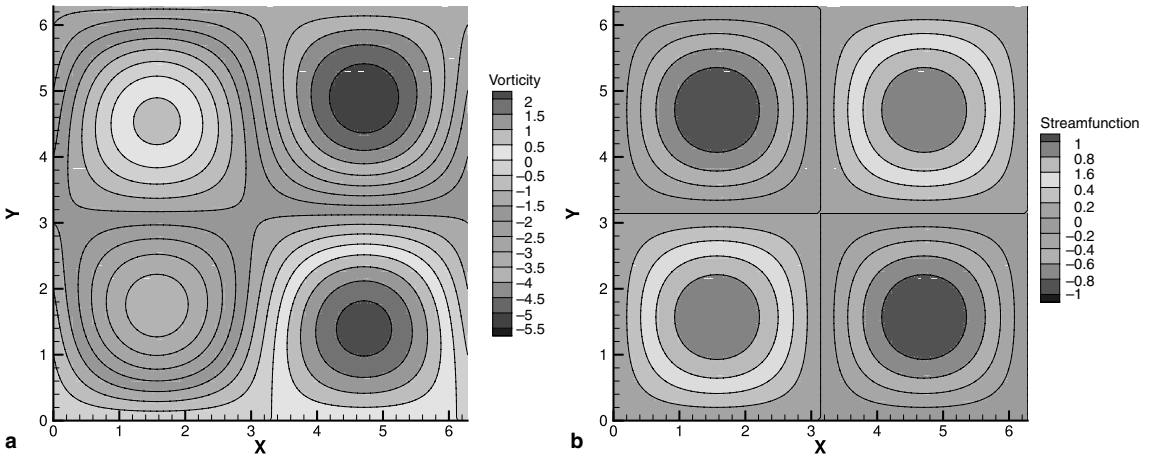

Fig. 4. (a) Potential vorticity and (b) streamfunction field at $t = 12\pi$ for the traveling wave.

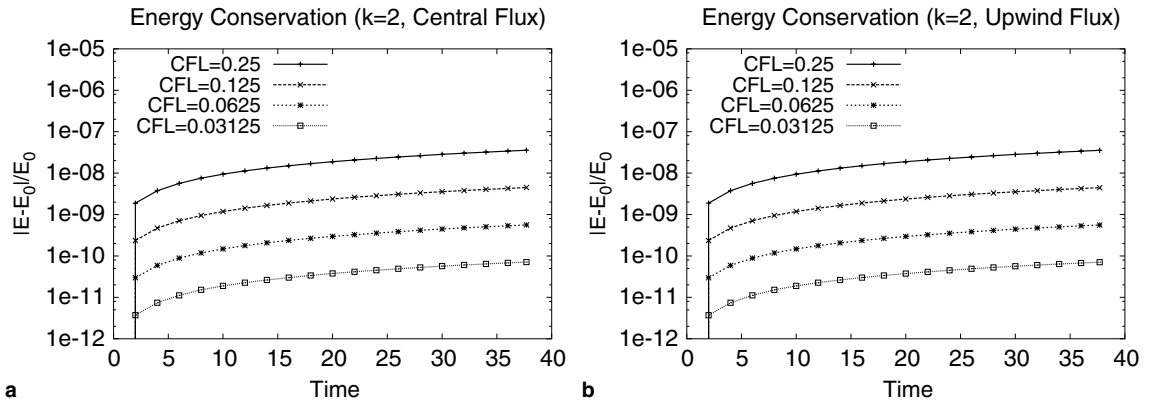

Fig. 5. The change in numerical energy $E = E_h$ (39), relative to the numerical energy, E_0, at $t = 0$, on a 32×32 grid using (a) a central flux (29a) and (b) an upwind flux (29b) for quadratic basis functions and for different time steps.

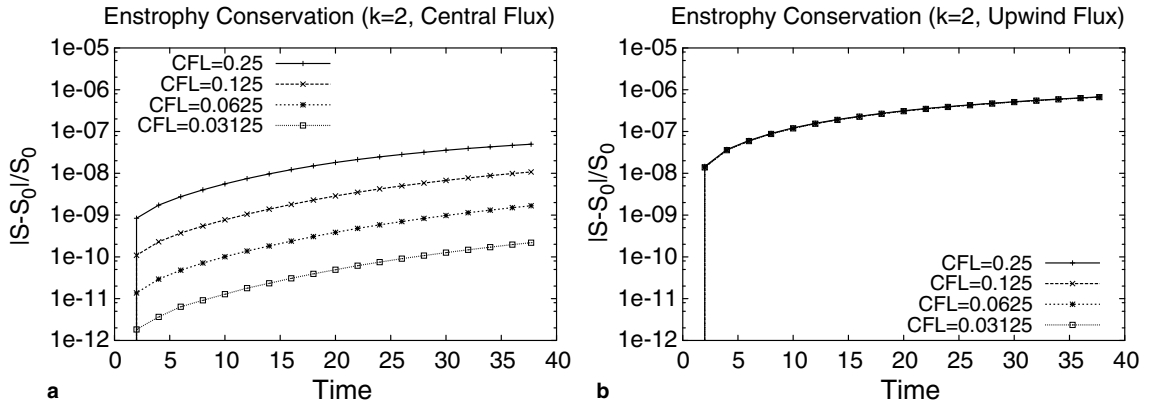

Fig. 6. The change in numerical enstrophy $S = S_h$ (44), relative to the numerical enstrophy, S_0, at $t = 0$, on a 32×32 grid using (a) a central flux and (b) an upwind flux for quadratic basis functions and for different time steps.

Table 10
Errors in ξ_h for the rigid lid example at $t = 8$ using the upwind flux

k	$\mathscr{T}_h$	L_1-error	Order	L_2-error	Order	L_∞-error	Order
1	8×8	3.18e − 01	–	1.19e − 01	–	1.97e − 01	–
	16×16	8.14e − 02	1.97	3.79e − 02	1.65	8.88e − 02	1.15
	32×32	1.92e − 02	2.09	8.70e − 03	2.12	2.45e − 02	1.86
	64×64	4.80e − 03	2.00	2.13e − 03	2.03	6.23e − 03	1.97
2	8×8	7.28e − 02	–	3.76e − 02	–	4.49e − 02	–
	16×16	8.73e − 03	3.06	5.21e − 03	2.85	8.45e − 03	2.41
	32×32	1.12e − 03	2.97	6.90e − 04	2.92	1.25e − 03	2.75
	64×64	1.41e − 04	2.98	8.78e − 05	2.97	1.61e − 04	2.96
3	8×8	1.36e − 02	–	5.70e − 03	–	1.09e − 02	–
	16×16	1.08e − 03	3.66	7.19e − 04	2.99	1.70e − 03	2.68
	32×32	5.73e − 05	4.23	4.33e − 05	4.05	1.89e − 04	3.17
	64×64	3.46e − 06	4.05	2.61e − 06	4.05	1.33e − 05	3.83

The L^1-, L^2- and L^∞-errors and orders of convergence for kth-order basis functions are shown.

Table 11
Errors in ξ_h for the rigid lid example at $t = 8$ using the central flux

k	$\mathscr{T}_h$	L_1-error	Order	L_2-error	Order	L_∞-error	Order
1	8×8	7.07e − 01	–	1.95e − 01	–	2.36e − 01	–
	16×16	2.35e − 01	1.59	6.93e − 02	1.49	7.46e − 02	1.66
	32×32	3.85e − 02	2.61	1.24e − 02	2.48	2.75e − 02	1.44
	64×64	7.34e − 03	2.39	2.57e − 03	2.27	7.03e − 03	1.97
2	8×8	3.05e − 01	–	8.15e − 02	–	7.71e − 02	–
	16×16	3.40e − 02	3.17	1.01e − 02	3.01	1.28e − 02	2.59
	32×32	4.28e − 03	2.99	1.23e − 03	3.04	1.55e − 03	3.04
	64×64	5.41e − 04	2.98	1.58e − 04	2.96	2.46e − 04	2.66
3	8×8	3.71e − 02	–	1.04e − 02	–	1.30e − 02	–
	16×16	4.26e − 03	3.12	1.27e − 03	3.03	2.02e − 03	2.68
	32×32	2.38e − 04	4.16	7.05e − 05	4.17	1.88e − 04	3.42
	64×64	1.34e − 05	4.15	4.09e − 06	4.11	1.33e − 05	3.83

The L^1-, L^2- and L^∞-errors and orders of convergence for kth-order basis functions are shown.

Table 12
Errors in ψ_h for the rigid lid example at $t = 8$ using the upwind flux

k	$\mathscr{T}_h$	L_1-error	Order	L_2-error	Order	L_∞-error	Order
1	8×8	4.48e − 01	–	2.19e − 01	–	2.55e − 01	–
	16×16	1.18e − 01	1.92	7.31e − 02	1.58	1.30e − 01	0.97
	32×32	2.98e − 02	1.99	1.84e − 02	1.99	4.01e − 02	1.70
	64×64	7.45e − 03	2.00	4.60e − 03	2.00	1.06e − 02	1.92
2	8×8	8.51e − 02	–	5.13e − 02	–	7.47e − 02	–
	16×16	9.18e − 03	3.21	5.68e − 03	3.18	1.08e − 02	2.79
	32×32	1.12e − 03	3.03	6.99e − 04	3.02	1.34e − 03	3.02
	64×64	1.42e − 04	2.99	8.80e − 05	2.99	1.68e − 04	3.00
3	8×8	1.36e − 02	–	5.92e − 03	–	1.06e − 02	–
	16×16	1.07e − 03	3.67	7.49e − 04	2.98	1.90e − 03	2.49
	32×32	5.71e − 05	4.23	4.36e − 05	4.10	1.98e − 04	3.26
	64×64	3.46e − 06	4.05	2.62e − 06	4.06	1.37e − 05	3.85

The L^1-, L^2- and L^∞-errors and orders of convergence for kth-order basis functions are shown.

Table 13
Errors in ψ_h for the rigid lid example at $t = 8$ using the central flux

k	$\mathcal{T}_h$	L_1-error	Order	L_2-error	Order	L_∞-error	Order
1	8×8	4.47e − 01	–	2.19e − 01	–	2.55e − 01	–
	16×16	1.19e − 01	1.92	7.36e − 02	1.57	1.33e − 01	0.94
	32×32	2.98e − 02	1.99	1.84e − 02	2.00	4.04e − 02	1.72
	64×64	7.45e − 03	2.00	4.60e − 03	2.00	1.06e − 02	1.93
2	8×8	8.64e − 02	–	5.23e − 02	–	7.51e − 02	–
	16×16	9.22e − 03	3.23	5.71e − 03	3.19	1.09e − 02	2.78
	32×32	1.12e − 03	3.04	6.99e − 04	3.03	1.34e − 03	3.03
	64×64	1.42e − 04	2.99	8.80e − 05	2.99	1.68e − 04	3.00
3	8×8	1.37e − 02	–	5.94e − 03	–	1.08e − 02	–
	16×16	1.07e − 03	3.67	7.50e − 04	2.99	1.90e − 03	2.51
	32×32	5.71e − 05	4.23	4.36e − 05	4.10	1.98e − 04	3.27
	64×64	3.46e − 06	4.05	2.62e − 06	4.06	1.37e − 05	3.85

The L^1-, L^2- and L^∞-errors and orders of convergence for kth-order basis functions are shown.

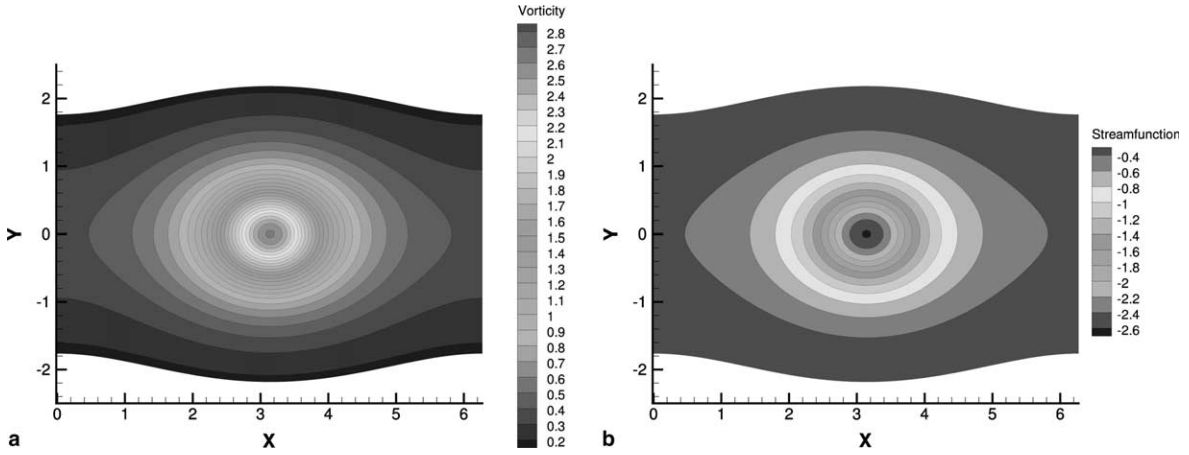

Fig. 7. (a) Vorticity and (b) streamfunction field at $t = 8$ for the rigid lid example.

8.3. Example 3: Rigid lid equations

Consider a modified solution of the Stuart vortex for the rigid lid equations (see Section 2 and Appendix A.3). The left and right boundary ($x = 0$ and $x = 2\pi$) are periodic. On the upper boundary we prescribe a value for the streamfunction, while at the lower boundary we prescribe a value of the circulation given by (57). The solutions are seen to converge to $O(h^k)$ and $O(h^{k+1})$ for the vorticity and streamfunction in Tables 10–13. Numerical results for the streamfunction and vorticity are shown in Fig. 7.

9. Summary and conclusion

To summarize, the following results have been obtained:

- A generalized (potential) vorticity streamfunction formulation was defined, including not only the incompressible 2D Euler equations as in [9], but also the quasi-geostrophic and rigid lid equations. This

formulation was shown to conserve energy and any weighted smooth function of the (potential) vorticity. In particular, enstrophy is conserved.

- Multiply connected and curved domains were considered, requiring the introduction of circulation around each connected piece of boundary and the use of isoparametric elements at curved boundaries for higher-order spatial discretizations. Otherwise, only a restricted set of initial conditions can be considered, and higher-order accuracy cannot be obtained as any local reduction of accuracy due to improper boundary elements affects the global solution of the streamfunction.
- The generalized system was discretized using a DG finite element method for the vorticity equation, and a continuous Galerkin finite element method for the elliptic equation to determine the streamfunction. Particular attention was paid to efficiently implement the circulation boundary condition, which requires use of the modified function space (17).
- The implementation of the numerical method matched the properties of conservation of numerical energy and enstrophy. Hence, the function space used in the continuous Galerkin discretization was a subset of the discontinuous one: $\mathsf{W}_h^k \subset \mathsf{V}_h^k$, which was also implemented and tested numerically. It is important to stress that for geophysical applications, preservation of at least energy and enstrophy is required and generally accepted practice for long-time integrations.
- An implicit time discretization scheme was defined for which conservation of energy and stability of enstrophy for the system discretized in space and time was proven, but not tested numerically.
- Three exact solutions, one for each of the above geophysical applications, were used to verify the numerical algorithm and implementation in curved and multiple connected domains. In these test cases, the explicit third-order Runge–Kutta time discretization was used. Particular attention was paid to observe the tendency towards energy conservation and L^2-stability.
- In accordance with our error estimates, the scheme was shown to converge, often an order higher than the $\mathrm{O}(h^k)$ predicted by the analysis for kth-order basis functions.

Further work will consist of extending the mixed continuous and DG finite element formulation to balanced equations in geophysical fluid dynamics (see, e.g. [12]), and simulations of localized nonlinear vortical flows around separatrices in complex, curved domains. In addition, a discontinuous (space-time) Galerkin finite-element discretization of both hyperbolic and elliptic equations with energy and enstrophy conservation and stability is of interest.

Acknowledgments

It is a pleasure to thank Dr. Ferenc Izsák for careful proofreading the manuscript. O.B. acknowledges a fellowship from The Royal Netherlands Academy of Arts and Sciences (KNAW).

Appendix A. Exact solutions

Exact solutions of (1) are given for the examples used in Section 8.

A.1. Stuart vortex

The Stuart vortex [15,6] is an exact stationary solution of the Euler equations (2) with:

$$\xi(x,y,t) = 1/(a\cosh y + \sqrt{a^2-1}\cos x)^2 \quad \text{and} \tag{A.1a}$$

$$\psi(x,y,t) = \log\left(a\cosh y + \sqrt{a^2-1}\cos x\right) \tag{A.1b}$$

with $a \geqslant 1$. The domain used in Section 8.1 is

$$\Omega = \{(x,y) \in \mathbb{R}^2 \mid 0 \leqslant x \leqslant 2\pi, \quad K_1 \leqslant \psi(x,y,0) \leqslant K_2\} \tag{A.2}$$

with $K_i = \log(ac_i + a + \sqrt{a^2-1})$ for $c_1 > 0$ and $-2\sqrt{a^2-a}/a < c_2 < 0$. We took $c_1 = -\sqrt{5}/2$, $c_2 = 2$ and $a = 3/2$. The left and right boundaries of the domain are periodic. The remaining parts of the boundary consist of three connected parts:

$$\partial\Omega_{\text{up}} = \{(x,y) \in \Omega \,|\, y \geqslant 0, \quad \psi(x,y,0) = K_2\}, \tag{A.3a}$$

$$\partial\Omega_{\text{down}} = \{(x,y) \in \Omega \,|\, y \leqslant 0, \quad \psi(x,y,0) = K_2\}, \tag{A.3b}$$

$$\partial\Omega_{\text{in}} = \{(x,y) \in \Omega \,|\, \psi(x,y,0) = K_1\}. \tag{A.3c}$$

A.2. Traveling wave example

A traveling wave solution for the quasi-geostrophic equations (3) is:

$$\xi(x,y,t) = -3\sin(x-ct)\sin(y) - y/2, \tag{A.4a}$$

$$\psi(x,y,t) = \sin(x-ct)\sin(y). \tag{A.4b}$$

In Section 8.2, the wave speed $c = 1/6$, and $A = B = 1$ and $D = -y/2$.

A.3. Rigid lid example

An exact stationary solution of the rigid lid equations (4) has been constructed based on the Stuart vortex. In (1), we take $B = 0$, $D = 0$ and

$$A = 1/H = a\cosh y + \sqrt{a^2-1}\cos x. \tag{A.5}$$

The stationary solution of the system is now given by

$$\xi(x,y,t) = -\psi(x,y,t) = 1/\left(a\cosh y + \sqrt{a^2-1}\cos x\right) \tag{A.6a}$$

with $a \geqslant 0$. In Section 8.3, $a = 3/2$. Note that the real velocity of the fluid (not the depth integrated velocity), given by $\vec{u} = (1/H)\nabla^{\perp}\psi$, is equal and opposite to the velocity of the Stuart vortex solution given in Section 8.1.

Appendix B. Proof of Theorem 11

In this appendix, we give a proof of the error estimate for the continuous–discontinuous Galerkin discretization for generalized vorticity dynamics, stated in Theorem 11.

We denote with Ω a bounded domain $\Omega \subset \mathbb{R}^2$ with Lipschitz boundary $\partial\Omega$. We define the Hilbert space $H^k(\Omega)$ of k-times weakly differentiable functions which are square integrable, including all derivatives up to the order k. The norm in $H^k(\Omega)$ is defined as $\|w\|_{H^k(\Omega)} = (\sum_{|\alpha|\leqslant k}\|D^{\alpha}w\|^2_{L^2(\Omega)})^{\frac{1}{2}}$ and the semi-norm as $|w|_{H^k(\Omega)} = (\sum_{|\alpha|=k}\|D^{\alpha}w\|^2_{L^2(\Omega)})^{\frac{1}{2}}$, with $L^2(\Omega) = H^0(\Omega)$. Here $D^{\alpha}w$ denotes the weak derivative of order $|\alpha|$ of w with α the multi-index symbol, see [4, Section 1.2]. For clarity we use in this section $\|w\|_{L^2(\Omega)}$ for the L^2 norm instead of $\|w\|_{\Omega}$ used elsewhere in this paper. The space of essentially bounded functions is denoted as $L^{\infty}(\Omega)$ and is equipped with the norm $\|w\|_{L^{\infty}(\Omega)} = \operatorname{ess\,sup}_{(x,y)\in\Omega}|w(x,y)|$. For any nonnegative integer m, $C^m(\Omega)$ denotes the space of all functions w which, together with all their partial derivatives $D^{\alpha}w$ of order

$|\alpha| \leqslant m$, are continuous in Ω. For $0 < \lambda \leqslant 1$, we define $C^{m,\lambda}(\overline{\Omega})$ to be the subspace of $C^m(\overline{\Omega})$, with $\overline{\Omega}$ the closure of Ω, consisting of those functions w for which for $0 \leqslant \alpha \leqslant m$, $D^\alpha w$ satisfies in Ω a Hölder condition of exponent λ, that is there exists a constant C such that

$$|D^\alpha w(x) - D^\alpha w(y)| \leqslant C|x-y|^\lambda, \quad \forall x, y \in \Omega.$$

Define the projection $P_K : H^{k+1}(\Omega) \mapsto \mathsf{V}_h^k$, with for each $K \in \mathscr{T}_h$

$$(P_K v, w/A)_K = (v, w/A)_K, \quad \forall w \in \mathsf{V}_h^k, \tag{B.1}$$

for which the following interpolation estimates are available:

$$\|\xi - P_K\xi\|_{H^1(K)} \leqslant C_I h^k |\xi|_{H^{k+1}(\tilde{K})}, \tag{B.2}$$

$$\|\xi - P_K\xi\|_{L^2(\partial K)} \leqslant C h^{k+1/2} \|\xi\|_{H^{k+1}(\tilde{K})} \tag{B.3}$$

with $\tilde{K}$ the patch of elements which connect to an edge or a vertex of element K. For a proof of (B.2) and (B.3), see Theorem 4.4 and Remark 8 in [2]. We also introduce the error in the vorticity and streamfunction, $\epsilon = \xi - \xi_h$ and $\delta = \psi - \psi_h$, respectively, and the projection of the vorticity error $\epsilon_h = P_K\epsilon = P_K\xi - \xi_h$.

The first step in the proof of Theorem 11 is to find a relation between the errors δ and ϵ. Using Theorem 5.6.8 in [4], we directly obtain a coercivity estimate for the bilinear form L defined in (19)

$$L(w,w) \geqslant \frac{1}{2} A_0 \|w\|^2_{H^1(\Omega)} - b\|w\|^2_{L^2(\Omega)}, \quad \forall w \in H^1(\Omega) \tag{B.4}$$

with $A_0 = \operatorname{ess\,inf}\{A(x,y) \,|\, (x,y) \in \Omega\} > 0$ and $b \geqslant \frac{1}{2}A_0 - B_0$, where $B_0 = \operatorname{ess\,inf}\{B(x,y) \,|\, (x,y) \in \Omega\}$.

If we subtract (22) from (18) then we obtain the following relation for the error in the streamfunction δ:

$$L(\delta, w) = -(\epsilon/A, w)_\Omega, \quad \forall w \in \mathsf{W}_h^k. \tag{B.5}$$

Taking $w = \delta$ in (B.5) and using the coercivity estimate for L, (B.4), we obtain

$$\begin{aligned}
\frac{1}{2} A_0 \|\delta\|^2_{H^1(\Omega)} &\leqslant L(\delta,\delta) + b\|\delta\|^2_{L^2(\Omega)} \\
&= -(\epsilon/A, \delta)_\Omega + b\|\delta\|^2_{L^2(\Omega)} && \text{(B.6)} \\
&\leqslant \|\epsilon/A\|_{L^2(\Omega)} \|\delta\|_{L^2(\Omega)} + b\|\delta\|^2_{L^2(\Omega)} && \text{(B.7)} \\
&\leqslant \frac{1}{2}\|\epsilon/A\|^2_{L^2(\Omega)} + \left(b + \frac{1}{2}\right)\|\delta\|^2_{L^2(\Omega)}. && \text{(B.8)}
\end{aligned}$$

In (B.6), we used the error equation (B.5), in (B.7) the Schwarz inequality and finally the arithmetic–geometric mean inequality in (B.8).

The next step is to provide an error bound for the $L^2(\Omega)$ norm of δ. For this we consider the adjoint equation

$$-\nabla \cdot (A\nabla w) + Bw = \phi \quad \text{in } \Omega \tag{B.9}$$

with $\phi \in L^2(\Omega)$, and

$$\hat{n} \cdot \nabla w = 0 \quad \text{at } \partial\Omega. \tag{B.10}$$

Then, for $w \in V$, with $V := H^1(\Omega)$ if $B \neq 0$ and $V := \{v \in H^1(\Omega) \,|\, \int_\Omega v \,\mathrm{d}\Omega = 0\}$ if $B = 0$, we obtain

$$(\delta, \phi)_\Omega = -(\delta, \nabla \cdot (A\nabla w))_\Omega + (\delta, Bw)_\Omega = L(\delta, w). \tag{B.11}$$

In (B.11) we use, respectively, (B.9), integrate by parts and apply the boundary condition (B.10). If we add now (B.5), where we denote $w \in \mathsf{W}_h^k$ as w_h, and (B.11) then we obtain

$$
\begin{aligned}
(\delta,\phi)_\Omega &= L(\delta, w-w_h) + (\epsilon/A, w-w_h)_\Omega - (\epsilon/A, w)_\Omega \\
&\leqslant C_{\mathrm{AB}}\|\delta\|_{H^1(\Omega)} \inf_{\chi\in W_h^k}\|w-\chi\|_{H^1(\Omega)} + \|\epsilon/A\|_{L^2(\Omega)} \inf_{\chi\in W_h^k}\|w-\chi\|_{L^2(\Omega)} + \|\epsilon/A\|_{L^2(\Omega)}\|w\|_{L^2(\Omega)} \\
&\leqslant C_{\mathrm{AB}}C_{\mathrm{I}}h\|\delta\|_{H^1(\Omega)}\|w\|_{H^2(\Omega)} + \|\epsilon/A\|_{L^2(\Omega)}(C_{\mathrm{I}}h^2+1)\|w\|_{H^2(\Omega)}
\end{aligned} \tag{B.12}
$$

with $C_{\mathrm{AB}} = \max(\|A\|_{L^\infty(\Omega)}, \|B\|_{L^\infty(\Omega)})$ and we used the Schwarz inequality in the second step, and finally the interpolation estimate Theorem 4.4.20, p. 109 in [4] with constant C_{I}. An upper bound for $\|w\|_{H^2(\Omega)}$ can be obtained using the fact that the differential operator in (B.9) is strongly elliptic, the related bilinear form L in (19) is a symmetric and coercive bilinear form on $H^1(\Omega)$, see (B.4), and using the regularity estimate given by Theorem 4.18(ii), pp. 137–138 in [11], where we assume that $A, B \in C^{m,1}(\overline{\Omega})$ with $m \geqslant 0$. This, together with the boundary condition (B.10), implies that

$$
\|w\|_{H^{m+2}(\Omega_1)} \leqslant C\|w\|_{H^1(\Omega_2)} + C\|\phi\|_{H^m(\Omega_2)}, \quad m \geqslant 0, \tag{B.13}
$$

where $\Omega_1 = G_1 \cap \Omega$, $\Omega_2 = G_2 \cap \Omega$, with G_1 and G_2 open subsets of $\mathbb{R}^2$ such that $\overline{G_1}$ is a compact subset of G_2. Here, G_1 intersects the boundary of Ω and G_2 has a smooth boundary not necessarily completely contained in Ω. An estimate for $\|w\|_{H^1(\Omega)}$ satisfying (B.9) together with the boundary condition (B.10) can be obtained directly from Theorem 4.10(i), pp. 128–129 in [11]. Introducing this result into (B.13) we obtain

$$
\|w\|_{H^{m+2}(\Omega)} \leqslant C_{\mathrm{R}}\|\phi\|_{H^m(\Omega)}, \qquad m \geqslant 0, \quad \forall w \in V, \tag{B.14}
$$

where we used that Ω can be covered by a finite number of sets Ω_1.

If we insert (B.14), with $m = 0$, into (B.12) and set ϕ equal to δ, then we obtain the estimate

$$
\|\delta\|_{L^2(\Omega)} \leqslant C_{\mathrm{I}}C_{\mathrm{R}}C_{\mathrm{AB}}h\|\delta\|_{H^1(\Omega)} + (C_{\mathrm{I}}h^2+1)C_{\mathrm{R}}\|\epsilon/A\|_{L^2(\Omega)}. \tag{B.15}
$$

Next, we combine (B.8) and (B.15) and use the arithmetic–geometric mean inequality which results in

$$
\frac{1}{2}A_0\|\delta\|^2_{H^1(\Omega)} \leqslant \left(\frac{1}{2} + (2b+1)C_{\mathrm{R}}^2(C_{\mathrm{I}}h^2+1)^2\right)\|\epsilon/A\|^2_{L^2(\Omega)} + (2b+1)C_{\mathrm{I}}^2C_{\mathrm{R}}^2C_{\mathrm{AB}}^2h^2\|\delta\|^2_{H^1(\Omega)}. \tag{B.16}
$$

Assume now that the mesh size $h \leqslant h_0$, with $(2b+1)C_{\mathrm{I}}^2C_{\mathrm{R}}^2C_{\mathrm{AB}}^2h_0^2 = \frac{1}{4}A_0$, or equivalently

$$
h_0 = \frac{\sqrt{A_0}}{C_{\mathrm{I}}C_{\mathrm{R}}C_{\mathrm{AB}}\sqrt{4(2b+1)}},
$$

which is the condition on h_0 stated in Remark 13, then we obtain the following relation between the errors δ and ϵ:

$$
\|\delta\|_{H^1(\Omega)} \leqslant \frac{2}{\sqrt{A_0}}\left(\frac{1}{2} + (2b+1)C_{\mathrm{R}}^2(C_{\mathrm{I}}h_0^2+1)^2\right)^{\frac{1}{2}}\|\epsilon/A\|_{L^2(\Omega)} = C_E\|\epsilon/A\|_{L^2(\Omega)}. \tag{B.17}
$$

Note, if $b + \frac{1}{2} \leqslant 0$ in (B.16), or equivalently $B_0 \geqslant \frac{1}{2}A_0 + \frac{1}{2}$, then $\frac{1}{2}A_0 - (2b+1)C_{\mathrm{I}}^2C_{\mathrm{R}}^2C_{\mathrm{AB}}^2h^2 \geqslant 0$ and there is no restriction on the minimum mesh size h_0 anymore, which proves Remark 14.

Consider now the error in the vorticity. Subtract (30) from (25) and use (1b), then the error equation for the vorticity is equal to

$$
(\partial_t\epsilon/A, v)_K = (\xi\nabla^\perp\psi - \xi_h\nabla^\perp\psi_h, \nabla v)_K - (\xi\nabla^\perp\psi\cdot\hat{n} - \hat{\xi}_h\nabla^\perp\psi_h\cdot\hat{n}, v^-)_{\partial K}, \qquad \forall K \in \mathscr{T}_h, \quad \forall v \in V_h^k, \tag{B.18}
$$

where the superscripts $-$ and $+$ in this section refer to the trace at the element boundary ∂K taken from the inside and outside of the element, respectively. Take $v = \epsilon_h$ and use that $(\partial_t \epsilon/A, v)_K = (\partial_t \epsilon_h/A, v)_K$ for each $v \in \mathsf{V}_h^k$ and $K \in \mathscr{T}_h$ to obtain

$$\frac{1}{2}\frac{\mathrm{d}}{\mathrm{d}t}(\epsilon_h/A, \epsilon_h)_\Omega = \sum_{K\in\mathscr{T}_h} \left(\xi \nabla^\perp \psi - \xi_h \nabla^\perp \psi_h, \nabla \epsilon_h\right)_K - \sum_{K\in\mathscr{T}_h} \left(\xi \nabla^\perp \psi \cdot \hat{n} - \hat{\xi}_h \nabla^\perp \psi_h \cdot \hat{n}, \epsilon_h^-\right)_{\partial K}. \tag{B.19}$$

Rewriting the first term on the right-hand-side of (B.19) results in

$$\begin{aligned}
\sum_{K\in\mathscr{T}_h} \left(\xi \nabla^\perp \psi - \xi_h \nabla^\perp \psi_h, \nabla \epsilon_h\right)_K &= \sum_{K\in\mathscr{T}_h} \left(\xi \nabla^\perp \delta + \epsilon \nabla^\perp \psi_h, \nabla \epsilon_h\right)_K \\
&= \sum_{K\in\mathscr{T}_h} \left\{ \left(\xi \nabla^\perp \delta, \nabla \epsilon_h\right)_K + \left(\epsilon \nabla^\perp \psi_h, \nabla \epsilon\right)_K - \left(\epsilon \nabla^\perp \psi_h, \nabla(\xi - P_K \xi)\right)_K \right\} \\
&= \sum_{K\in\mathscr{T}_h} \left\{ -\left(\epsilon_h \nabla^\perp \delta, \nabla \xi\right)_K + \left(\xi \epsilon_h^-, \nabla^\perp \delta \cdot \hat{n}\right)_{\partial K} + \frac{1}{2}\left((\epsilon^-)^2, \nabla^\perp \psi_h \cdot \hat{n}\right)_{\partial K} \right. \\
&\quad \left. - \left(\epsilon \nabla^\perp \psi_h, \nabla(\xi - P_K \xi)\right)_K \right\}.
\end{aligned} \tag{B.20}$$

Plugging this result into (B.19) gives

$$\begin{aligned}
\frac{1}{2}\frac{\mathrm{d}}{\mathrm{d}t}(\epsilon_h/A, \epsilon_h)_\Omega &= -(\epsilon_h, \nabla^\perp \delta \cdot \nabla \xi)_\Omega - \sum_{K\in\mathscr{T}_h} \left(\epsilon, \nabla^\perp \psi_h \cdot \nabla(\xi - P_K \xi)\right)_K \\
&\quad + \sum_{K\in\mathscr{T}_h} \left\{ \left(\epsilon_h^- \xi, \nabla^\perp \delta \cdot \hat{n}\right)_{\partial K} + \frac{1}{2}\left((\epsilon^-)^2, \nabla^\perp \psi_h \cdot \hat{n}\right)_{\partial K} - \left(\xi \nabla^\perp \psi \cdot \hat{n} - \hat{\xi}_h \nabla^\perp \psi_h \cdot \hat{n}, \epsilon_h^-\right)_{\partial K} \right\}.
\end{aligned} \tag{B.21}$$

Define $\hat{\epsilon} = \xi - \hat{\xi}_h$ and rewrite the boundary terms in (B.21) as follows:

$$\begin{aligned}
&\sum_{K\in\mathscr{T}_h} \left\{ \left(\epsilon_h^- \xi, \nabla^\perp \delta \cdot \hat{n}\right)_{\partial K} + \frac{1}{2}\left((\epsilon^-)^2, \nabla^\perp \psi_h \cdot \hat{n}\right)_{\partial K} - \left(\xi \nabla^\perp \psi \cdot \hat{n} - \hat{\xi}_h \nabla^\perp \psi_h \cdot \hat{n}, \epsilon_h^-\right)_{\partial K} \right\} \\
&\quad = \sum_{K\in\mathscr{T}_h} \left(\frac{1}{2}(\epsilon^-)^2 - \epsilon^- \hat{\epsilon}, \nabla^\perp \psi_h \cdot \hat{n}\right)_{\partial K} + \sum_{K\in\mathscr{T}_h} \left(\hat{\epsilon}(\xi - (P_K \xi)^-), \nabla^\perp \psi_h \cdot \hat{n}\right)_{\partial K}
\end{aligned} \tag{B.22}$$

to obtain

$$\begin{aligned}
\frac{1}{2}\frac{\mathrm{d}}{\mathrm{d}t}(\epsilon_h/A, \epsilon_h)_\Omega = &- \underbrace{\left(\epsilon_h, \nabla^\perp \delta \cdot \nabla \xi\right)_\Omega}_{\text{(A)}} - \underbrace{\textstyle\sum_{K\in\mathscr{T}_h} \left(\epsilon, \nabla^\perp \psi_h \cdot \nabla(\xi - P_K \xi)\right)_K}_{\text{(B)}} \\
&+ \underbrace{\textstyle\sum_{K\in\mathscr{T}_h} \left(\frac{1}{2}(\epsilon^-)^2 - \epsilon^- \hat{\epsilon}, \nabla^\perp \psi_h \cdot \hat{n}\right)_{\partial K}}_{\text{(C)}} + \underbrace{\textstyle\sum_{K\in\mathscr{T}_h} \left(\hat{\epsilon}(\xi - (P_K \xi)^-), \nabla^\perp \psi_h \cdot \hat{n}\right)_{\partial K}}_{\text{(D)}}.
\end{aligned} \tag{B.23}$$

Now, we evaluate the terms (A), (B), (C) and (D) separately. For (A), we apply the Schwarz inequality, the relation $\|\nabla^\perp \delta\|_{L^2(\Omega)} = \|\nabla \delta\|_{L^2(\Omega)}$ and use (B.17), with $\epsilon = \epsilon_h + \xi - P_K \xi$, followed by the arithmetic–geometric mean inequality

$$\begin{aligned}
(\epsilon_h, \nabla^\perp \delta \cdot \nabla \xi)_\Omega &\leqslant \|\nabla \xi\|_{L^\infty(\Omega)} \|\epsilon_h\|_{L^2(\Omega)} \|\nabla \delta\|_{L^2(\Omega)} \\
&\leqslant C_E \|\nabla \xi\|_{L^\infty(\Omega)} \|\epsilon_h\|_{L^2(\Omega)} \left(\|\epsilon_h/A\|_{L^2(\Omega)} + \|(\xi - P_K \xi)/A\|_{L^2(\Omega)}\right) \\
&\leqslant C \|\nabla \xi\|_{L^\infty(\Omega)} \left(\frac{3}{2}\|\epsilon_h\|_{L^2(\Omega)}^2 + \frac{1}{2}\|\xi - P_K \xi\|_{L^2(\Omega)}^2\right).
\end{aligned} \tag{B.24}$$

For (B), we use the regularity estimate Theorem 4.18(i), pp. 137–138 in [11]. Together with the boundary condition $\psi = c_D(t)$ at $\partial\Omega_D$ (7), and the condition $A, B \in C^{m,1}(\overline{\Omega})$, this implies that

$$\|\psi\|_{H^{m+2}(\Omega_1)} \leqslant C\|\psi\|_{H^1(\Omega_2)} + C\|\xi\|_{H^m(\Omega_2)} + c_D(t)\left(\int_{\Gamma_2} \mathrm{d}S\right)^{\frac{1}{2}}, \quad m \geqslant 0 \tag{B.25}$$

with $\Gamma_2 = \partial\Omega \cap \Omega_2$. An estimate for $\|\psi\|_{H^1(\Omega)}$ satisfying (19)–(20) together with the boundary condition (7) can be obtained directly from Theorem 4.10 (i), pp. 128–129 in [11]. Introducing this result into (B.25) together with the inequality showing that $c_D(t)$ is bounded in terms of the vorticity (see [16]) we obtain

$$\|\psi\|_{H^{m+2}(\Omega)} \leqslant C\|\xi\|_{H^m(\Omega)}, \qquad m \geqslant 0, \quad \forall \psi \in V, \tag{B.26}$$

where we used that Ω can be covered by a finite number of sets Ω_1. Since $H^2(\Omega)$ is embedded in $L^\infty(\Omega)$ (Theorem 4.12 [1], p. 85) and using the regularity estimate (B.26) this also implies

$$\begin{aligned}\|\nabla^\perp \psi_h\|_{L^\infty(\Omega)} &\leqslant \|\nabla^\perp \delta\|_{L^\infty(\Omega)} + \|\nabla^\perp \psi\|_{L^\infty(\Omega)} \leqslant \|\nabla^\perp \delta\|_{L^\infty(\Omega)} + C\|\psi\|_{H^3(\Omega)} \\ &\leqslant \|\nabla^\perp \delta\|_{L^\infty(\Omega)} + C\|\xi\|_{H^1(\Omega)}\end{aligned} \tag{B.27}$$

for $A, B \in C^{1,1}(\overline{\Omega})$. We also have the relation

$$\begin{aligned}\|\nabla^\perp \delta\|_{L^\infty(\Omega)} &= \|\nabla(\psi - \psi_h)\|_{L^\infty(\Omega)} \leqslant \|\nabla(\psi - P_\Omega \psi)\|_{L^\infty(\Omega)} + \|\nabla(P_\Omega \psi - \psi_h)\|_{L^\infty(\Omega)} \\ &\leqslant Ch|\psi|_{H^3(\Omega)} + Ch^{-1}\|\nabla(P_\Omega \psi - \psi_h)\|_{L^2(\Omega)} \\ &\leqslant Ch\|\xi\|_{H^1(\Omega)} + Ch^{-1}\left(\|\nabla\delta\|_{L^2(\Omega)} + \|\nabla(\psi - P_\Omega\psi)\|_{L^2(\Omega)}\right) \\ &\leqslant Ch\|\xi\|_{H^1(\Omega)} + Ch^{-1}\|\delta\|_{H^1(\Omega)}, \qquad m \geqslant 0, \quad h > 0\end{aligned} \tag{B.28}$$

with P_Ω a global Lagrangian interpolant. In the second inequality, we use a standard interpolation estimate for P_Ω (Theorem 4.4.20 in [4]) and an inverse inequality (Theorem 4.5.11 in [4]). Next, we use the regularity estimate (B.26) and the triangle inequality, and, finally, for $\|\nabla(\psi - P_\Omega\psi)\|_{L^2(\Omega)}$ the interpolation estimate Theorem 4.4.20 in [4] and (B.26) again. Combining (B.27) and (B.28) and using (B.17), we obtain the estimate

$$\|\nabla^\perp \psi_h\|_{L^\infty(\Omega)} \leqslant C\left(\|\xi\|_{H^1(\Omega)} + \frac{1}{h}\|\epsilon\|_{L^2(\Omega)}\right), \quad 0 < h \leqslant 1$$

and apply the Schwarz inequality to obtain

$$\begin{aligned}\sum_{K\in\mathscr{T}_h} \left(\epsilon, \nabla^\perp \psi_h \cdot \nabla(\xi - P_K\xi)\right)_K &\leqslant \sum_{K\in\mathscr{T}_h} \|\nabla^\perp \psi\|_{L^\infty(K)}\|\epsilon\|_{L^2(K)}\|\nabla(\xi - P_K\xi)\|_{L^2(K)} \\ &\leqslant C\|\xi\|_{H^1(\Omega)} \sum_{K\in\mathscr{T}_h} \|\nabla(\xi - P_K\xi)\|_{L^2(K)}\left(\|\epsilon_h\|_{L^2(K)} + \|\xi - P_K\xi\|_{L^2(K)}\right) \\ &\quad + C\sum_{K\in\mathscr{T}_h} \frac{1}{h}\left(\|\epsilon_h\|_{L^2(K)} + \|\xi - P_K\xi\|_{L^2(K)}\right)^2 \|\nabla(\xi - P_K\xi)\|_{L^2(K)} \\ &\leqslant C\|\xi\|_{H^1(\Omega)} \sum_{K\in\mathscr{T}_h} \left(\|\epsilon_h\|^2_{L^2(K)} + \|\xi - P_K\xi\|^2_{H^1(K)}\right) \\ &\quad + C\sum_{K\in\mathscr{T}_h} h^{k-1}\|\xi\|_{H^{k+1}(K)}\left(\|\epsilon_h\|^2_{L^2(K)} + \|\xi - P_K\xi\|^2_{L^2(K)}\right) \\ &\leqslant C\|\xi\|_{H^{k+1}(\Omega)} \sum_{K\in\mathscr{T}_h} \left(\|\epsilon_h\|^2_{L^2(K)} + \|\xi - P_K\xi\|^2_{H^1(K)}\right), \qquad k \geqslant 1, \quad 0 \leqslant h \leqslant 1,\end{aligned} \tag{B.29}$$

where the geometric mean inequality and the interpolation estimate (B.2) are used in the third step. For (C), we use the stability condition (28) and the relation $\hat{\epsilon} = \bar{\epsilon} - (\hat{\xi}_h - \bar{\xi}_h)$ with $\bar{\xi}_h = (1/2)(\xi_h^+ + \xi_h^-)$ and $\bar{\epsilon} = (1/2)(\epsilon^+ + \epsilon^-)$ to obtain

$$\begin{aligned}\sum_{K\in\mathscr{T}_h}\left(\frac{1}{2}(\epsilon^-)^2 - \epsilon^-\hat{\epsilon}, \nabla^\perp\psi_h\cdot\hat{n}\right)_{\partial K} &= -\frac{1}{2}\underbrace{\sum_{K\in\mathscr{T}_h}\left(\epsilon^-\epsilon^+, \nabla^\perp\psi_h\cdot\hat{n}\right)_{\partial K}}_{=0} + \sum_{K\in\mathscr{T}_h}\left(\epsilon^-(\hat{\xi}_h - \bar{\xi}_h), \nabla^\perp\psi_h\cdot\hat{n}\right)_{\partial K}\\ &= \frac{1}{2}\sum_{K\in\mathscr{T}_h}\left((\epsilon^- - \epsilon^+)(\hat{\xi}_h - \bar{\xi}_h), \nabla^\perp\psi_h\cdot\hat{n}\right)_{\partial K}\\ &= \frac{1}{2}\sum_{K\in\mathscr{T}_h}\left((\xi_h^+ - \xi_h^-)(\hat{\xi}_h - \bar{\xi}_h), \nabla^\perp\psi_h\cdot\hat{n}\right)_{\partial K} \overset{(28)}{\leqslant} 0. \end{aligned} \tag{B.30}$$

For estimating (D), we use that for the upwind flux (29b) and central flux (29a) the following holds $\|\hat{\epsilon}\|_{L^2(\partial K)} \leqslant C(\|\epsilon^-\|_{L^2(\partial K)} + \|\epsilon^+\|_{L^2(\partial K)})$. Also using the trace theorem $\|\nabla^\perp\psi_h\|_{L^\infty(\partial K)} \leqslant C\|\nabla^\perp\psi_h\|_{L^\infty(K)}$ and the Schwarz inequality (D) then becomes

$$\begin{aligned}\sum_{K\in\mathscr{T}_h}\left(\hat{\epsilon}(\xi - (P\xi)^-), \nabla^\perp\psi_h\cdot\hat{n}\right)_{\partial K} &\leqslant C\sum_{K\in\mathscr{T}_h}\|\nabla^\perp\psi_h\|_{L^\infty(K)}\|\xi - (P_K\xi)^-\|_{L^2(\partial K)}\|\hat{\epsilon}\|_{L^2(\partial K)}\\ &\leqslant C\sum_{K\in\mathscr{T}_h}\left(\|\xi\|_{H^1(K)} + \frac{1}{h}\|\epsilon\|_{L^2(K)}\right)\|\xi - (P_K\xi)^-\|_{L^2(\partial K)}\\ &\quad\times\left(\|\epsilon^+\|_{L^2(\partial K)} + \|\epsilon^-\|_{L^2(\partial K)}\right)\\ &\leqslant C\|\xi\|_{H^{k+1}(\Omega)}\sum_{K\in\mathscr{T}_h}\left(\|\xi - (P_K\xi)^-\|_{L^2(\partial K)} + h^{k-\frac{1}{2}}\left(\|\epsilon_h\|_{L^2(K)} + \|\xi - P_K\xi\|_{L^2(K)}\right)\right)\\ &\quad\times\left(\|\epsilon_h^+\|_{L^2(\partial K)} + \|\xi - (P_K\xi)^+\|_{L^2(\partial K)} + \|\epsilon_h^-\|_{L^2(\partial K)} + \|\xi - (P_K\xi)^-\|_{L^2(\partial K)}\right)\end{aligned} \tag{B.31}$$

with $h \leqslant 1$. In the last step we used the interpolation inequality (B.3). Assuming that the mesh is quasi uniform, we can combine Lemma 4.5.3 in [4] and Theorem 1.6.6 in [4] to obtain the following inverse inequality:

$$\|v^-\|_{L^2(\partial K)} \leqslant \frac{C}{\sqrt{h}}\|v\|_{L^2(K)}, \quad \forall v \in \mathsf{V}_h^k.$$

Applying this estimate for $v = \epsilon_h$ to (B.31) and using the arithmetic–geometric mean inequality results, under the condition $0 \leqslant h \leqslant 1$ and $k \geqslant 1$, in

$$\sum_{K\in\mathscr{T}_h}\left(\hat{\epsilon}(\xi - (P_K\xi)^-), \nabla^\perp\psi_h\cdot\hat{n}\right)_{\partial K} \leqslant C\|\xi\|_{H^{k+1}(\Omega)}\sum_{K\in\mathscr{T}_h}\left\{\frac{1}{h}\|\xi - (P_K\xi)^-\|_{L^2(\partial K)}^2 + \|\xi - (P_K\xi)^-\|_{L^2(K)}^2 + \|\epsilon_h\|_{L^2(K)}^2\right\}. \tag{B.32}$$

Combining the above estimates for (A), (B), (C) and (D), plugging them into (B.23), and using the interpolation estimates (B.2) and (B.3) results in

$$\frac{1}{2}\frac{\mathrm{d}}{\mathrm{d}t}\|\epsilon_h\|_{L^2(\Omega)}^2 \leqslant C\sup_{t\in[0,T]}\left(\|\nabla\xi(\cdot,t)\|_{L^\infty(\Omega)}, \|\xi(\cdot,t)\|_{H^{k+1}(\Omega)}\right)\left(\|\epsilon_h\|_{L^2(\Omega)}^2 + h^{2k}\|\xi\|_{H^{k+1}(\Omega)}^2\right)$$

with $k \geqslant 1$ the polynomial order of the basis functions and $0 \leqslant h \leqslant 1$. Now we use the Gronwall inequality, which states that if $y \geqslant 0$ satisfies $\mathrm{d}y(t)/\mathrm{d}t \leqslant C(y(t) + h(t))$ for $0 \leqslant t \leqslant T$ with C a constant, $h(t) \geqslant 0$ and $h \in L^1([0,T])$ then $y(t) \leqslant \exp(CT)\{y(0) + \int_0^T h(s)\,\mathrm{d}s\}$. Hence, we find for $t \in [0,T]$ that

$$\|\epsilon_h\|^2_{L^2(\Omega)} \leqslant \exp\left(CT \sup_{t\in[0,T]} (\|\nabla\xi(\cdot,t)\|_{L^\infty(\Omega)}, \|\xi(\cdot,t)\|_{H^{k+1}(\Omega)})\right)\left(\left[\|\epsilon_h\|^2_{L^2(\Omega)}\right]_{t=0} + h^{2k}\int_0^T \|\xi(\cdot,t)\|^2_{H^{k+1}(\Omega)}\,\mathrm{d}t\right),$$
$$k \geqslant 1.$$

If we apply for each element $K \in \mathscr{T}_h$ the projection P_K given by (B.1) to the initial condition and use the interpolation estimate (B.2) then

$$\left[\|\epsilon_h\|_{L^2(\Omega)}\right]_{t=0} \leqslant Ch^k\|\xi(\cdot,0)\|_{H^k(\Omega)}$$

with $k \geqslant 1$, and thus for $t \in [0,T]$ we obtain

$$\|\epsilon_h\|_{L^2(\Omega)} \leqslant Ch^k \exp\left(CT \sup_{t\in[0,T]} (\|\nabla\xi(\cdot,t)\|_{L^\infty(\Omega)}, \|\xi(\cdot,t)\|_{H^{k+1}(\Omega)})\right)\left(\|\xi(\cdot,0)\|^2_{H^k(\Omega)} + \int_0^T \|\xi(\cdot,t)\|^2_{H^{k+1}(\Omega)}\,\mathrm{d}t\right)^{\frac{1}{2}},$$

with $k \geqslant 1$.

The error in the vorticity can now be estimated using the relation

$$\|\epsilon\|_{L^2(\Omega)} \leqslant \|\epsilon_h\|_{L^2(\Omega)} + \|\xi - P_K\xi\|_{L^2(\Omega)} \leqslant \|\epsilon_h\|_{L^2(\Omega)} + h^k \sup_{t\in[0,T]} \|\xi(\cdot,t)\|_{H^{k+1}(\Omega)}, \tag{B.33}$$

where in the second step we use the interpolation estimate (B.2). An estimate for the total error is obtained by combining (B.17) and (B.33) and using (1b), viz., $\vec{u} = A\nabla^\perp\psi$, $\vec{u}_h = A\nabla^\perp\psi_h$, which implies $\|\vec{u} - \vec{u}_h\|_{L^2(\Omega)} \leqslant C\|\psi - \psi_h\|_{H^1(\Omega)} = C\|\delta\|_{H^1(\Omega)}$, and completes the proof. □

The proof of Corollary 12 follows directly from (B.28).

References

[1] R.A. Adams, J.J.F. Fournier, Sobolev Spaces, second ed., Academic Press, New York, 2003.
[2] C. Bernardi, V. Girault, A local regularization operator for triangular and quadrilateral finite elements, SIAM J. Numer. Anal. 35 (5) (1998) 1893.
[3] E. Bernsen, O. Bokhove, J.J.W. van der Vegt, Additional technical appendices to this article. Memorandum, Mathematical Communications, Department of Applied Mathematics, University of Twente, ISSN 0169-2690, 2005.
[4] S.C. Brenner, L.R. Scott, The Mathematical Theory of Finite Element Methods, Springer, New York, 1994.
[5] E. Hairer, C. Lubich, G. Wanner, Geometric Numerical Integration, Springer, New York, 2002.
[6] D. Holm, J.E. Marsden, T. Ratiu, Non-linear stability of the Kelvin–Stuart cat's eyes flow, Lect. Appl. Math. 23 (1986) 171.
[7] L.D. Landau, E.M. Lifschitz, Fluid Mechanics, Pergamon Press, New York, 1959.
[8] P.H. LeBlond, L.A. Mysak, Waves in the Ocean, Elsevier, Amsterdam, 1978.
[9] J. Liu, C.-W. Shu, A high-order discontinuous Galerkin method for 2D incompressible flows, J. Comput. Phys. 160 (2000) 577.
[10] E.N. Lorenz, Energy and numerical weather prediction, Tellus 12 (1960) 364.
[11] W.C.H. McLean, Strongly Elliptic Systems and Boundary Integral Equations, Cambridge University Press, Cambridge, 2000.
[12] M.E. McIntyre, W.A. Norton, Potential vorticity inversion on a hemisphere, J. Atmos. Sci. 57 (2000) 1214.
[13] J. Pedlosky, Geophysical Fluid Dynamics, Springer, Berlin, 1979.
[14] C.-W. Shu, S. Osher, Efficient implementation of essentially non-oscillatory shock-capturing schemes, J. Comput. Phys. 77 (1988) 439.
[15] J.T. Stuart, On finite amplitude oscillations in laminar mixing layers, J. Fluid Mech. 29 (1967) 417.

[16] J.J.W. van der Vegt, F. Iszák, O. Bokhove, Error analysis of a continuous–discontinuous Galerkin finite element method for generalized 2D vorticity dynamics. Memorandum 1759, Department of Applied Mathematics, University of Twente, 2005 (online available).
[17] J. Yan, C.-W. Shu, A local discontinuous Galerkin method for KdV type equations, SIAM J. Numer. Anal. 40 (2002) 769.